The Pennsylvania State University

The Graduate School

College of Engineering

A STUDY ON THE ELECTROLYTIC DECOMPOSITION OF HAN-BASED PROPELLANTS FOR MICROTHRUSTER APPLICATIONS

A Thesis in

Mechanical Engineering

by

Bo-Han Kuo

Submitted in Partial Fulfillment

of the Requirements

for the Degree of

Master of Science

December 2010

The thesis of Bo-Han Kuo was reviewed and approved by the following*:

Richard A. Yetter
Professor of Mechanical Engineering
Thesis Co-Advisor

Jongguen Lee
Senior Research Associate of Mechanical Engineering
Thesis Co-Advisor

Kenneth K. Kuo
Distinguished Professor of Mechanical Engineering

Karen A. Thole
Head of the Department of Mechanical and Nuclear Engineering

*Signatures are on file in the Graduate School

ABSTRACT

The characteristics of electrolytic decomposition of HAN-based liquid propellants including 13M HAN and HAN269MEO15 were investigated in a single channel liquid flow reactor which consists of a straight electrolytic channel and a combustion chamber adjacent to it. Both metal (Stainless Steel 316) and Low Temperature Co-Fired Ceramic (LTCC) reactors were designed and fabricated for complementary types of experiments. Visual observation was made to observe the two-phase flow inside the electrolytic channel of the optically-accessible metal reactor and the evolution of product species was attained in the Low Temperature Co-Fired Ceramic reactors to study the decomposition process of HAN-based propellants.

The liquid propellants were decomposed into warm gases with temperature ~300^{o}C in LTCC reactors when a voltage of 30-50VDC was applied across the electrolytic channel. The initial condensed-phase reaction was observed to be followed by the gas-phase reaction base upon the species evolution and the temperature profile. Major species detected included N_2O, NO, and NO_2 (in order of decreasing concentration) in 13M HAN decomposition and N_2O and CH_3ONO in HAN269MEO15 decomposition. A high temperature reaction of HAN269MEO15 was initiated in the combustion chamber loaded with catalyst S 405. The reaction was found to be dominated by electrolytic decomposition at low temperature with major species N_2O and CH_3ONO and dominated by catalytic reaction at high temperature with major species NO, CO_2, and CO indicating a more complete reaction.

TABLE OF CONTENTS

LIST OF FIGURES

LIST OF TABLES

ACKNOWLDGEMENTS

I would like to express my sincerest gratitude to my co-advisors Dr. Richard A. Yetter and Dr. Jongguen Lee for their continuous guidance, support, and encouragement. I would like to thank them for giving me the opportunity to work on this project. The experience and knowledge I have gained from their guidance throughout this work is invaluable. I would like to sincerely thank Dr. Kenneth K. Kuo for his time and effort in reviewing this thesis.

I would also like to thank Ms. Amanda Baker at Material Research Lab for her assistance and insightful inputs in fabricating LTCC reactors. I would like to thank Mr. Larry Horner for his professional technical assistance in machining, and Ms. Mary Newby, Mr. John Raiser, and Ms. Ginny Smith for their excellent administrative assistance. I would like to thank all the members of Dr. Yetter's research group for their help and assistance in research.

I am grateful to the AFOSR for funding this project. Gratitude is also extended to Dr. Ronald A. Spores at Aerojet for providing the catalyst employed in this study as well as his invaluable suggestions. Collaboration and discussion with Dr. Kuo-Cheng Lin of Taitech, Inc. are also greatly appreciated.

Finally, I would like to thank my friends for being with me through those sunny days and stormy nights during my study here. I would like thank my parents and my sister for their never ending love and prayers.

Chapter 1 Introduction

1.1 Background and Motivation

To reduce launch costs and risks and increase the functionality of space missions, efforts have been made toward the miniaturization of satellites and spacecraft within government and industry since the 1980s [1]. Within the U.S. and European space communities, microspacecrafts are defined as spacecrafts having a mass less than 100 kg. The propulsion system used in a microspacecraft is referred to as the micropropulsion system [1]. Applications of micropropulsion are not limited to microspacecraft, but can be extended to any situations where a low thrust level or impulse bit is required, such as for actuation, pumping microfluids, morphing surfaces, etc. To enable microspacecraft applications and other advanced space missions, micropropulsion system must not only meet requirements for thrust and impulse bit levels but also stringent physical constraints of microspacecraft including limitations on volume, mass, power, and bus voltage.

Chemical propulsion and electric propulsion find their own roles in micropropulsion applications because of their distinctive characteristics. Chemical propulsion is said to be "energy constrained" [2] since the energy required to accelerate the exhaust gases to produce thrust is from the chemical energy released by the exothermic reaction of propellants. The propulsion performance is accordingly limited by the chemical energy stored in the propellants. While in electric propulsion, it is the electric energy which is usually converted from solar energy or nuclear energy that accelerate the propellant. Although solar energy and nuclear energy is almost unlimited in space, the power

delivered is limited by the size of an electric energy conversion unit. Consequently, electric propulsion is said to be "power constrained." Based on their limiting factors, chemical propulsion is always preferred if a higher thrust is required or when the power is limited while electric propulsion is more suitable when a finer impulse bit or a longer operation time is needed or possible [3-4].

Chemical propulsion has been investigated for micropropulsion applications based upon cold gas, solid propellant, bipropellant, and monopropellant technologies. Hydrazine has been the state-of-the-art monopropellant technology since its debut in 1966[5]. It is extensively used in attitude control and primary propulsion for small spacecraft because of the simplicity of propellant delivery and propulsion systems and its ignition reliability. However, its toxic nature requires special ground handling and operating procedures, and also poses potential health hazards to personnel. Recently, "green propellants" including hydrogen peroxide and some weakly energetic ionic liquids such as hydroxylammonium nitrate (HAN), hydrazinium nitroformate (HNF), and ammonium dinitramide (ADN) started to receive considerable attention due to their low toxicity [5]. Among these candidate propellants, HAN-based propellants are the most advanced and have the potential to provide a promising alternative to hydrazine based on previous studies in literature [6-8]. In the current study, hydroxylammonium nitrate (HAN)-based monopropellants are being investigated.

The major challenges encountered during the development of HAN-based propellants include combustion instability, reliability of ignition and suitable high temperature materials [4-8]. Catalytic ignition has been used in hydrazine thruster operation and

provides an easy and reliable ignition while no catalyst has been identified yet to have spontaneous reaction with HAN-based propellants where preheating is always required to get an acceptable ignition. To attain a comparable specific impulse with hydrazine, the operating temperature of HAN-based propellants which is adjustable by changing the composition of the propellant mixture, needs to be higher than that of hydrazine because of the higher average molecular weight of the combustion products of HAN-based propellants. The more energetic the HAN-based propellant composition is, the shorter the survivability of the structure and catalyst would be. The utilization of high-temperature materials is thus required. In addition, the more complex ignition and combustion characteristics of the HAN-based propellants compared to hydrazine requires more efforts in experimentation to attain a better understanding of the controlling processes and consequently the development process is slower.

The feasibility of utilizing electrolytic decomposition either as a primary ignition method or as a precursory step prior to catalyst ignition is studied in the current work. HAN-based propellant is decomposed into warm gases through electrolysis. By passing the product gases from electrolytic decomposition through a catalyst bed, high temperature reaction is expected to be initiated without preheating the catalytic chamber. By depositing the ignition energy directly into propellant as electric energy instead of to the structure as heat, the system should be more energy efficient particularly in small thruster systems where the heat loss is always significant.

1.2 Goals and Approach

The goals of the current work have been to obtain better understandings of the process of electrolytic decomposition of HAN-based propellants, and then investigate the feasibility of combining electrolysis with catalytic ignition in thruster operation. Such ignition methods can serve as an alternative to preheated catalytic ignition. Furthermore, under circumstances where gas generated from electrolysis is sufficiently rapid, direct pressurization may be possible with restriction at the exit of the reactor such that a catalyst is not required.

In order to achieve these goals, the following approach was taken. Firstly, the characteristics of electrolytic decomposition of HAN-based propellants were studied. Visual observations of electrolytic decomposition of HAN-based propellants were made to observe the two-phase flow in the electrolytic microchannel of the optically-accessible metal reactor. The evolution of reaction temperature combined with the analysis of product species via Fourier Transform Infrared Spectrometer (FTIR) instrument helped obtain a better understanding of the reaction process. The difference between thermal and electrolytic decomposition of HAN-based propellants was compared. With these information attained from experiments, a better understanding of the process of electrolytic decomposition of HAN-based propellants was expected to be gained. After investigating the characteristics of electrolytic decomposition of HAN-based propellants, electrolytic decomposition of HAN-based propellants was combined with catalytic ignition to prove the ability to achieve a high temperature reaction at atmospheric pressure.

Chapter 2 Literature Review

Hydroxylammonium nitrate (HAN), the nitrate salt of hydroxylamine with chemical formula NH_3OHNO_3, is a solid at room temperature and melts at 48^oC [9]. It can be mixed with water up to a concentration of 95% to make a salt mixture in ionic form with cation NH_3OH^+ and anion NO_3^-.

HAN, by itself, could undergo exothermic decomposition when proper activation energy is provided while the excess of oxygen in HAN makes it suitable as an oxidizer. HAN-based propellants which consist of HAN as the oxidizer, and fuel and water, as the solvent and stabilizer have long been considered as potential propellants in liquid gun propulsion and rocket propulsion. The properties and energy content of the propellant can be altered by adjusting the amount of water and utilizing different fuels depending on the required performance. More recently, HAN-based propellants were also proposed as monopropellants for thruster application and often seen as a potential candidate as an alternative to hydrazine because of its low toxicity and high energy density over the state-of- the-art monopropellant hydrazine.

2.1 Combustion Studies

2.1.1 Staged Combustion Characteristics

Compared to other monopropellants with only one single component like hydrazine or hydrogen peroxide, the ignition and combustion processes of HAN-based propellants

are more complex because of the multi-component property. One of the most significant characteristics of HAN-based propellant combustion is that it happens in steps. The sequence of the reaction was revealed through visual observations of combustion behaviors as well as analysis of the product species using different diagnostic techniques. Different models describe these characteristics were proposed as will be discussed in the following sections.

Klein [10] described the combustion of HAN-based propellants containing triethanol ammonium nitrate (TEAN) as the fuel component as a three-stage reaction: (1) Initiation, (2) ignition, and (3) combustion. The whole reaction is initiated by the decomposition of HAN in condensed-phase producing heat and gases (including H_2O, N_2O, N_2, NO, NO_2, and HNO_3). A spray of molten TEAN droplets was also produced in this stage. The "ignition" stage started as TEAN droplet started to become involved in the reaction and more heat was released so that the reaction could be self sustained. The final stage was defined as "combustion" where most of the energy stored in the propellant is released. Vosen [11] suggested the combustion of LP 1846 (see Table 2.1 for composition) occurred in two stages: (1) Exothermic decomposition of HAN in condensed-phase and (2) gas-phase reaction between the product of HAN decomposition and TEAN.

2.1.2 Combustion Phenomena

The understanding of the combustion characteristics of HAN-based propellants is necessary prior to its application in propulsion systems. Strand burner tests of HAN-based propellants over a range of pressures were conducted to investigate the combustion

behaviors and reaction rates and their dependence on pressure [11-15]. A high power CO_2 laser was utilized to achieve full ignition of one HAN-based propellant to examine combustion behaviors and the pertinent combustion chemistry at atmospheric pressure [16]. The major findings are discussed below in more detail.

Vosen [12] observed a luminous flame in the strand burner tests of LP1846 when the pressure was higher than 26.7MPa. The luminous flame was positioned above a transparent zone referred to as a dark zone in nitramine propellants on top of the liquid-gas interface which was identified as the reaction front. At lower pressures, no visible flame was observed. The transparent zone became opaque as pressures were lowered. The different reaction zones observed in the strand burner are one indication of the staged-combustion characteristics. Chang and Kuo [14] observed the same phenomena as Vosen in strand burner tests of XM 46, which was formerly referred to as LP1846. A luminous flame appeared when the pressure was higher than 28MPa while the reaction was not self-sustainable at pressures lower than 1.82MPa. Different reaction zones were seen in the strand burner and the growth and decline of each reaction zone at different pressures is shown in Figure 2.1.The measured time-temperature profiles were able to be associated with different combustion stages. At a relatively low pressure of 13.8MPa where no flame appeared, the temperature measured in the dark opaque zone was around 300^{o}C. The start of the clearing of the dark opaque gases at different pressures corresponded to a temperature of 600^{o}C. At 33.8 MPa, the appearance of the luminous flame caused a sudden rise of temperature to 1700^{o}C. Chang et al. [13] suggested that the opaque gases might include brown-colored NO_2 and some heavy carbon-containing intermediate species. The

temperature rose to a higher level when the opaque gases disappeared into transparent species, and the reaction subsequent to the transparent species finally produced the luminous flame, where most of the chemical energy in the propellant was released.

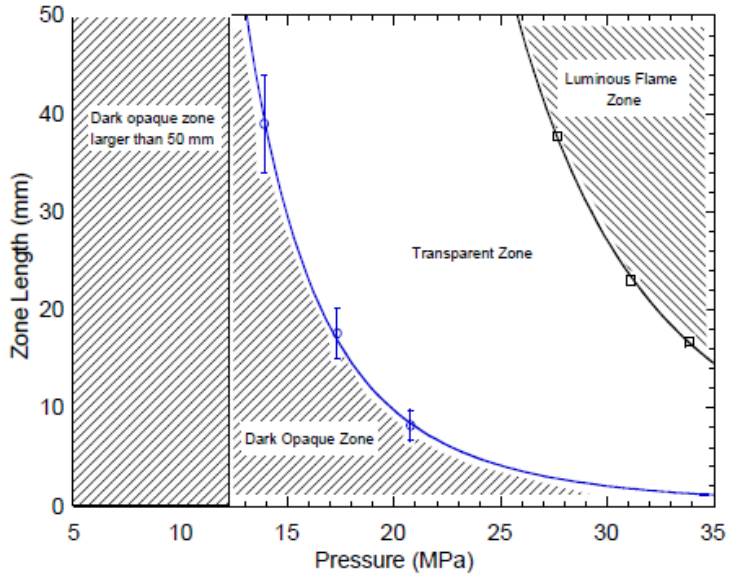

Figure 2.1 The growth and decline of different reaction zones over pressures [13]

In addition to XM 46, Chang et al. [14-15] also studied the combustion characteristics of other HAN-based propellants including HANGLY26, HAN269MEO15, and HAN284MEO17 (see Table 2.1 for their compositions) which were developed by Aerojet (formerly Primex) [6-7]. For HANGLY26, no luminous flame was observed over the pressures tested from 1.5 to 18.2 MPa. For pressures between 1.5 and 8.8MPa, bubbles were seen at the liquid-gas interface. A dark-cloud region appeared on top of liquid-gas interface and a translucent brown-colored gas was formed above the dark-cloud region. For pressures between 8.8 and 18.2 MPa, the size of bubbles at the liquid-gas interface decreased to an indiscernible level and the rest of the strand tube was filled by the

dark-cloud region. For strand burner tests carried out at lower than 8.7 MPa, the temperature finally leveled off at the boiling point of water after the reaction front had passed. At 8.7MPa, the temperature rose up to 400^{o}C as the translucent gas was produced. For HAN269MEO15, dark colored products were formed on top of liquid-gas interface at pressures between 1.21 and 6.4 MPa. The dark colored products were ignited and a luminous flame was evident only if the nichrome wire used for ignition of the liquid propellant was still heated. For pressures between 0.74 and 1.14 MPa, dark colored products were formed on top of liquid-gas interface. Above the dark colored product was the translucent brown gas which was similar to that of HANGLY26 over the pressures range 1.5 to 8.8MPa. The measured temperatures were confined between the boiling point of methanol and water after the reaction front had passed. Totally different combustion behaviors were shown for HAN284MEO17, which had a similar equivalence ratio but less water compared to HAN269MEO15. At pressures between 3.5 and 7.3 MPa, luminous flames were observed. Cyclic flame behaviors which were composed of purple, blue, white, blue, and purple flames in sequence were found near the lower end of this pressure range. At pressures between 0.9 and 2.9 MPa, a dark zone was observed which produced a brown translucent gas immediately.

Table 2.1 Composition of various HAN-based propellants studied by Vosen [12] and Chang et al. [13-15]

	HAN	AN	Water	Fuel
LP 1846	60.8wt%	N/A	20.0 wt%	TEAN 19.2 wt%
LP 1845	63.2 wt%	N/A	16.8 wt%	TEAN 20.0wt%
XM46	60.8wt%	N/A	20.0 wt%	TEAN 19.2 wt%
HANGLY26	60.0 wt %	N/A	26.0 wt%	Glycine 14.0 wt%
HAN269MEO15	69.7 wt%	0.60 wt%	14.91 wt%	Methanol 14.79 wt%
HAN284MEO17	77.25 wt%	0.67 wt%	4.89 wt%	Methanol 17.19 wt%

Lee and Litzinger [16] conducted laser assisted combustion experiments in air and argon and luminous flames of XM-46, 13M HAN, and solid TEAN were observed with a high power CO_2 laser at a heat flux of 400W/cm^2 at atmospheric pressure. The high heating rate was used to simulate the heat feedback from the gaseous reaction above the liquid surface in the actual combustion phenomena. For 13M HAN solution, a brown gas appeared after water boiled away, which subsequently ignited to generate a luminous flame (white in air, bright yellow in argon). TEAN originally in its solid phase, melted first and then emitted dark gas followed by the appearance of a luminous blue and then yellow flame indicating fuel-rich combustion in an air environment. As for XM-46 combustion, flames similar to that of HAN and TEAN appeared sequentially indicating staged combustion characteristics.

From the results of the strand burner experiments reported in the literature as summarized above, high pressure favors the completion of the combustion of HAN-based propellants while only early stages of reaction were triggered at lower pressure. The important role water plays in the HAN-based propellant combustion can be seen as the boiling point of water acted as a barrier that the reaction could not go beyond under some test conditions. Also, the totally different combustion characteristics between the two HAN/methanol propellants showed how the amount of water in the propellants can make a significant difference.

2.1.3 Burning Rates

The burning rates of HAN-based propellants have shown different dependences on pressure in different pressure regimes [11-15, 17]. From results of a liquid residue analysis attained under different pressures [4-5], the slope break points on the burning rate versus pressure plots coincided with changes in species concentration versus pressures indicating that the change of pressure dependence on burning rates is associated with a change of reaction mechanism. As shown in Figure 2.2, the burning rates of propellants with different compositions differed from each other.

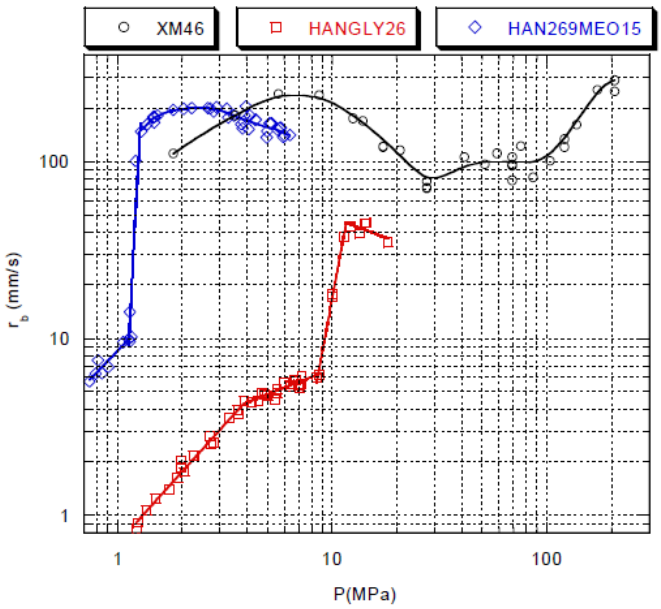

Figure 2.2 Burning rates of different HAN-based propellants [17]

Chang et al. [15] pointed out one possible cause for the rough combustion and pressure spikes observed in thruster operation reported by Aerojet [7] when operating at pressures in the same range where the burning rate of the propellant was observed to increase abruptly might be the nature of instable combustion of the propellant rather than the degradation of the catalyst from high combustion temperature.

2.2 Thermal Decomposition of HAN Based Propellants

2.2.1 Thermal Analysis

An accelerating rate calorimeter (ARC) was used to identify the exotherms in thermal decomposition of LG 1845 (see Table 2.1 for composition) [18]. Three separate exotherms

were seen at 122°C, 180°C, and 227°C which were attributed to the thermal decomposition of hydroxylammonium ion, nitrate ion, and triethonalammonium ion, respectively.

Thermal analysis techniques including thermogravimetric analysis (TGA) and differential thermal analysis (DTA) were applied to study the thermal decomposition of HAN solutions with various concentrations [19]. As shown in Figure 2.3, the endothermic evaporation of water was followed by the onset of exothermic reaction where decomposition product gas was formed. The onset of exothermic decomposition was found to be delayed to a higher temperature with a larger amount of water in the propellant.

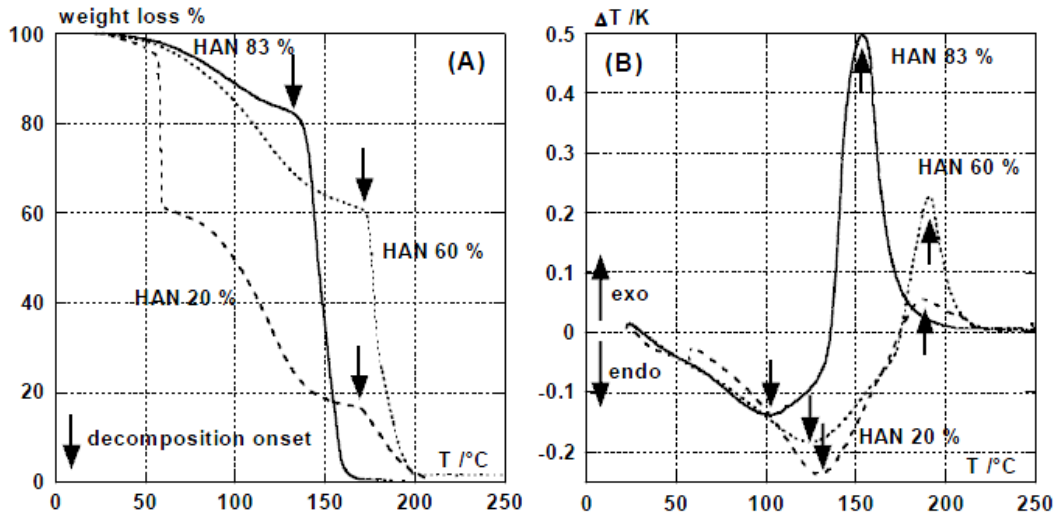

Figure 2.3 TGA (left) and DTA (right) results of thermal decomposition of HAN-water mixtures with different concentrations [19].

2.2.2 Species Evolution

The understanding of the species evolution throughout the decomposition of HAN-based propellants can lead to a better understanding of chemical kinetics and

reaction mechanism of the decomposition process. The decomposition products of XM 46, LP1845 and their components including solid HAN/ HAN solutions and TEAN were studied using FTIR through thermolysis [20-21] and TQ-MS in laser assisted combustion experiments [16]. The results of the species evolution of HAN-based propellants decomposition may vary from experiment to experiment depending on the test conditions including temperature, pressure, heating rates, fuel components, and even the sensitivity of the instrument. However, based on the results of temporal product species measurement, the reaction of the liquid propellants could still be generalized as a sequence of events which started with the evaporation of water followed by the HAN-dominated reaction and then the TEAN-dominated reaction [16, 21].

Typically, H_2O was the first detected species indicating the first event in the decomposition of the liquid propellants is the evaporation of water which concentrates the condensed propellants at the same time. The second event is mainly the decomposition of HAN possibly with partial reaction of TEAN. The major species decomposed are similar to those in the decomposition of HAN solutions and include N_2O, NO, NO_2, N_2 and HNO_3 with H_2CO, CO_2, CO, and HCN from the partial TEAN reaction. NO_2 was suggested to be formed from HNO_3 since it started to appear after the disappearance of HNO_3 [21]. The next event is the TEAN- dominated reaction where carbon- containing species rapidly increased and more heat is released. The major species detected from this stage include CO_2, CO, H_2O, N_2, NO, HCN and CH_3CN [16].

It was found that the reaction between HAN and TEAN in XM 46 occurred during early stage as indicated by the detection of carbon containing gases even prior to attaining

the decomposition temperature of TEAN, where no gas was detected below this point during thermal decomposition of TEAN alone [20-21]. A change in the species evolution rate also suggested the presence of reaction between HAN and TEAN in XM 46 when comparing with the thermolysis of HAN or TEAN alone [16, 20-21].

The effect of pressure on thermal decomposition of HAN-based propellants was also investigated in the thermolysis of LGP1845 [20]. Tests were carried out at 15 psi Ar, 200 psi Ar, 500 psi Ar, and 1000 psi Ar where a larger amount of CO_2, which is an indication of more complete combustion, was observed in experiments at higher pressures. The results again confirm the positive effect of pressure on the completion of the reaction.

2.3 Catalytic Decomposition

Primex (now a division of Aerojet) scientists conducted a series of tests in search of proper catalyst for HAN-based propellants in thruster applications [6-8]. Some proprietary Aerojet catalysts and thermally conditioned Shell 405 were found to perform well with no degradation or spikes in chamber pressure over 1000 seconds of life test time when testing with a low temperature HAN-glycine monopropellant [6]. S 405 (formerly Shell 405) consists of Iridium (31-33%) as the active material deposited on alumina substrate which has a maximum working temperature 1423K [22]. To find a suitable catalyst for high performance HAN-based blends which would have a combustion temperature up to 2422K, tests were performed with some high temperature ceramics used as catalyst carriers [8]. An Aerojet in-house catalyst, LCH233 (with the active material Iridium), despite its low surface area compared to S 405, was found to have reliable ignition, long endurance

(longer than 5 minutes) and multiple starts (more than 20 times) without significant degradation when testing with fuel-rich, oxidizer-rich, and stoichiometric high performance HAN-methanol propellants.

Courthéoux et al. [23] did a series of experiments to evaluate the performance of different catalysts in initiating the decomposition of HAN-based propellants and HAN solutions. Various substrate carriers including alumina, zirconia, barium, magnesium, and zirconium aluminate and active materials including some noble and non-noble metals have been tested. Different catalyst preparation methods were found to affect the activity and stability of the catalysts. The supports alone (either alumina or silica-doped alumina) without the active phase were shown to lower the onset decomposition temperature. With Platinum as the active material, catalytic decomposition could be initiated at a low temperature (<40^{o}C) with a delay time less than 1 second. However, iridium supported on alumina (36 wt % Ir/Al_2O_3) which is used to decompose Hydrazine was found to have a higher onset temperature of 98^{o}C suggesting this catalyst would not be the best choice if initiation at low temperature is desired.

2.4 Electric Ignition and Electrolytic Ignition

The electric ignition of HAN-based propellants in gun propulsion was extensively investigated by Army [24-25]. The original attempt was to ignite the propellants by arc discharge, in which the applied voltage was up to around 2000 volts. Under these conditions, it was found that electric energy was transferred to the propellants through ohmic heating and electrolytic or electrochemical processes prior to the occurrence of the

arc discharge [24]. To avoid the attrition of electrodes by arc discharge, arc-less ignition was also investigated and demonstrated to be feasible; i.e., the propellants were able to be ignited solely by ohmic heating and electrolytic reaction. Electric ignition was also used in the strand burner tests conducted by Vosen [12] where an electric capacitive discharge ranging from 200 to 1100 volts was used to ignite the HAN-based propellants through tantalum electrodes immerged in the liquid propellant.

Research on electrolytic ignition of liquid propellants in rocket propulsion has been limited. The concept of electrolytic ignition of liquid propellants in rocket propulsion was firstly shown in a patent in the 1970s [26]. The propellants had to be an "electrolytically dissociatable fluid monopropellant." As mentioned in the patent, hydrazine-hydrazine azide mixture was one of the potential candidates. The propellant was ignited using a voltage ranging from 2 to 30 volts applied across the electrodes and the reaction would continue even after the power was turned off.

The ionic structure of hydroxylammonium nitrate makes electrolytic decomposition or ignition of HAN-based propellants possible. The precursory electrolysis of HAN-based propellants by 6V battery was found to greatly enhance the decomposition of propellants in initiation of ignition by focused laser beams [27]. The characteristics of electrolytic ignition of HAN-based propellants were first examined with droplet tests at atmospheric pressure [28]. A droplet with diameter 1.5-2 millimeters was suspended by a bead at the end of a quartz fiber and nichrome or platinum wires with diameter of 250 μm were inserted into the droplet to serve as electrodes. The bubbling, gasification, and decomposition of XM 46 and HAN269MEO15 were observed when an electrical potential

ranging from 4 to 12 volts was applied. The application of higher voltages was found to shorten the time required to gasify the droplet. A microfin electrode module was also built to investigate the electrolytic characteristics of XM 46 [29]. The microfin electrode, which consisted of an array of titanium fins having a distance of 1 mm apart, was submerged into a beaker filled with propellant at atmospheric pressure. A voltage ranging from 7 to 12 volt was applied. The propellant was observed to bubble immediately once the voltage was applied and the liquid temperature measured in the beaker increased rapidly as the power was turned on. Power was turned off when the peak current which corresponded to the peak reactivity of the propellant was achieved. The reaction would propagate down the beaker and the temperature of the evolved gas continued to increase at a slower rate even after the power was off until cold water was added to dilute the propellant to quench the reaction. A typical temperature profile is shown in Figure 2.4. At atmospheric pressure, no second-stage reaction was observed in the electrolytic decomposition of HAN-based propellants; the highest temperature recorded in the liquid propellant was just 115^{o}C regardless of the voltage supplied which was close to the thermal decomposition temperature of HAN. It was also found that the ignition delay which was defined as the time required to attain the peak current was shorter and the total electric energy consumed was smaller when a higher voltage was applied. The authors thus made the conclusion that the rate of energy supplied was more important to the decomposition of the propellant than the amount of energy.

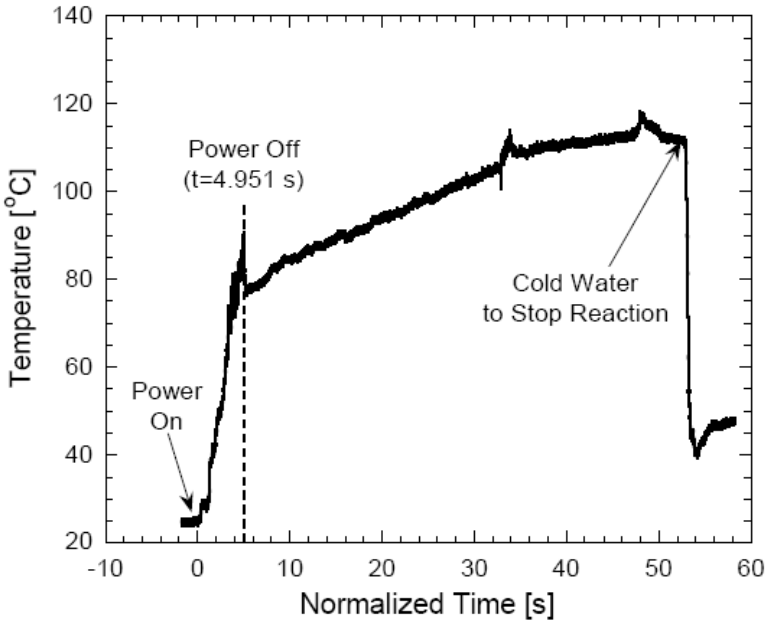

Figure 2.4 A typical temperature profile in the electrolytic decomposition test performed by Risha et al. [29]

A 2D single-shot thruster using low temperature co-fired ceramic tape technology was designed for electrolytic ignition of HAN–based propellants [30]. Liquid propellant was filled in the thrust chamber before firing. Full ignition of propellant as indicated by the luminous emission from the thruster body and the plume, was observed for voltages higher than 40 volts. A maximum thrust of 197 mN and an ignition delay of 1.881 s were measured when RK 315A was used as propellant and a voltage of 45 volts was applied while no detailed information about exit temperature and chamber pressure was provided in the paper.

2.5 Reaction Mechanism

2.5.1 Thermal Decomposition

Two reaction mechanisms of condensed-phase reactions of HAN were proposed based on previous reaction studies and experimental results [10, 31]. Lee and Litzinger [32] summarized and compared these two reaction mechanisms (Table 2.2) and constructed a reduced reaction model from them in order to deduce the Arrhenius-type reaction rates for HAN decomposition.

Table 2.2 Summary of reaction mechanisms of HAN condensed-phased reaction [32]

	Klein [10]	Oxley and Brower [31]
Initiate Reaction	$HAN \rightarrow NH_2OH + HNO_3$ $NH_2OH + HNO_3 \rightarrow HONO + HNO + H_2O$	$HAN \rightarrow NH_2OH + HNO_3$ $NH_2OH + HNO_3 \leftrightarrow HONO + HNO + H_2O$
N_2O Formation	$NH_3OH^+ + HONO$ $\rightarrow H_3O^+ + O = N - NH - OH$ $\leftrightarrow HO - N = N - OH$ $\rightarrow N_2O + H_2O$	$NH_2OH + HONO \leftrightarrow N_2O + 2H_2O$
N_2 Formation	$NH_3OH^+ + HNO \rightarrow N_2 + H_2O + H_3O^+$	$NH_2OH + HNO \rightarrow N_2 + 2H_2O$
Major NO Formation	None	None
NO_2 Formation	$HONO + HNO_3 \rightarrow 2NO_2 + H_2O$ $2HONO \rightarrow NO + NO_2 + H_2O$	None
Other Reaction	$HNO + NO_3^- \rightarrow HONO + NO_2^-$	$HNO + HNO_3 \rightarrow 2HONO$

It's generally agreed that the decomposition of HAN-based propellants is initiated with the endothermic proton transfer reaction ($HAN \rightarrow NH_2OH + HNO_3$) in the condensed-phase followed by the reaction between NH_2OH and HNO_3 to form HNO,

HONO, and water where HNO and HONO are very reactive. The reaction paths for the formation of gaseous products following the initiate reaction can also be seen in Table 2.2. The major difference between the reaction mechanisms proposed by Klein [10] and Oxley and Brown [31] is that Klein proposed NH_3OH^+ reacting with HONO and HNO to form N_2 and N_2O through an acid-catalyzed reaction which is more probable at a high acidity while Oxley and Brown suggested NH_2OH react with HONO and HNO to form N_2 and N_2O.

In the reduced reaction model constructed by Lee and Litzinger [32], another possible reaction path for the formation of N_2O from the dimerization of HNO was proposed: $2HNO \rightarrow N_2O + H_2O$ in addition to the above mentioned mechanisms. The dimerization of HNO to form N_2O is only of minor importance compared with the reaction between NH_2OH and HONO to form N_2O because a smaller HNO concentration compared to NH_2OH in the condensed-phase reaction of HAN. To account for a higher NO concentration compared to NO_2 observed in previous experiments, the reaction path for the formation of NO was also added in their model as: $3HONO \rightarrow 2NO + HNO_3 + H_2O$.

2.5.2 Electrolytic Decomposition

Some reaction paths were proposed [28, 33] for the electrolytic decomposition of HAN in additional to the reaction paths in thermal decomposition since the reaction mechanism in condensed-phase is expected to be altered by electrolytic reaction. Yetter et al. [28] mentioned any competing mechanisms to the proton transfer reaction which initiates the following exothermic reaction in thermal decomposition of HAN should lower

the reaction temperature and increase the reaction rate. Several possible competing reactions based on the electrolysis of water were suggested as follows [28, 33]:

At the anode:

$2H_2O \rightarrow O_2 + 4H^+ + 4e^-$

$H^+ + NH_3OH^+NO_3^- \text{ (HAN)} \rightarrow NH_3OH^+ + HNO_3$

$H^+ + NO_3^- \rightarrow HNO_3$

At the cathode:

$2NH_3OH^+ + 2e^- \rightarrow 2NH_2OH + H_2$

$2H_2O + 2e^- \rightarrow H_2 + 2OH^-$

$OH^- + NH_3OH^+NO_3^-(HAN) \rightarrow NH_2OH + H_2O + NO_3^-$

$OH^- + NH_3OH^+ \rightarrow NH_2OH + H_2O$

$NO_3^- + 4H^+ + 3e^- \rightarrow NO + 2H_2O$

$2H_2O + O_2 + 4e^- \rightarrow 4OH^-$

The electrolytic decomposition of HAN-based propellants was studied numerically with the incorporation of the proposed electrochemical mechanism of electrolytic decomposition [33] of HAN-based propellants as shown below to the existing reaction scheme of thermal decomposition of HAN proposed by Lee et al. mentioned earlier [32]. The individual reactions were represented as overall reactions at the anode and cathode.

At the anode:

$2(NH_3OH)^+(NO_3)^- + H_2O \rightarrow \frac{1}{2}O_2 + 2HNO_3 + 2(NH_3OH)^+ + 2e^-$

At the cathode:

$$2(NH_3OH)^+ + 2e^- \rightarrow 2NH_2OH + H_2$$

The global reaction arising from electrolytic decomposition thus becomes:

$$2(NH_3OH)^+(NO_3)^- + H_2O \rightarrow 2HNO_3 + 2NH_2OH + H_2 + \frac{1}{2}O_2$$

In addition to the advantage of a lower onset temperature in electrolytic decomposition of HAN-based propellants, the additional formation of hydrogen and oxygen was said to enhance the ignition and combustion [33].

However, rigorous experimental results for electrolytic decomposition of HAN which are required to gain an in-depth understanding of the combined-electrolytic and thermal reaction mechanism were still unavailable in literature. One of the objectives of the current work is thus to attain additional information on the species generated during the electrolytic decomposition to further understand the reaction mechanism.

2.6 Laboratory Thruster Operation

Laboratory thrusters were designed, built, and tested for HAN-based propellants to demonstrate the feasibility of in-space application [6-8, 34]. Catalytic ignition with a preheating temperature between 600-800^{o}F (588-700 K) was mainly used to get a reliable ignition and shorter ignition delay.

Some lower energy content formulations were tested and reliable ignition and clean, stable combustion were obtained. An Isp in the range of 190-195 seconds was determined experimentally as the theoretic Isp is 204 seconds [6]. The development and test of higher performance propellants were also pursued [7]. A 1-lbf laboratory thruster with thermally

conditioned Shell 405 catalyst was preheated to 800F (700K) before test firing. Six propellants as listed in Table 2.3 were found to have good handling, ignition, and combustion characteristics. However, the utilization of high temperature materials either for the thruster body or catalyst is required to survive the high combustion temperature of the high performance propellants. For the state-of-the-art catalyst for hydrazine, S 405 (formerly Shell 405) which could also be used in HAN application, the maximum working temperature is only 1150^{o}C (1423K) [35]. The degradation of the catalyst in the high performance propellant test firing was possibly the cause of the spikes in chamber pressure [7]. Some advanced catalyst materials were tested with high performance propellants [8]. With a preheated (to 400 ^{o}C) Aerojet in-house catalyst, LCH233, a measured specific impulse of 250 s was achieved with methanol blends.

Table2.3 Specific impulse and combustion temperature of promising high performance HAN-based propellants [7]

	Theoretical Isp (s)	Combustion Temperature (K)	Oxidizer (wt%)	Fuel (wt%)	Water (wt%)	Ammonium Nitrate (wt%)
HAN250GLY	250	2038	HAN 63.63%	Glycine 22.22%	13.61%	0.54%
HAN264GLY	264	2259	HAN **	Glycine **	**	**
HAN269MEO	269	2202	HAN 69.15%	Methanol 15.46%	14.79%	0.59 %
HAN253MEO	253	1724	HAN **	Methanol **	**	**
HAN284MEO	284	2422	HAN 77.25%	Methanol 17.19%	4.89%	0.67%
HAN278HEH	278	2370	HAN **	HEHN* **	**	**

*HEHN- Hydroxyethylhydrazinium Nitrate

**Data on composition not available

Chapter 3 Experiment Approach

3.1 Propellant Preparation

In the current work, electrolytic decomposition of two types of HAN-based mixtures including 13M HAN solution and HAN269MEO15 were studied. The composition of both propellants is shown in Table 3.1. The 13M HAN solution was provided by Arch Chemicals, Inc. The propellant, HAN269MEO15, was prepared by mixing 85.2wt% of 13M HAN solution with 14.8 wt% of reagent-grade methanol manufactured by J. T. Baker. HAN269MEO15 is considered as one of the high performance HAN-based propellants developed by Aerojet [7] which has an equivalence ratio of 0.95, an adiabatic flame temperature of 3504^{o}F (2202K), and a theoretical vacuum Isp value of 269 seconds.

Table 3.1 Compositions of 13M HAN and HAN269MEO15

	Water (wt %)	HAN (wt %)	Methanol (wt %)
13M HAN	18	82	N/A
HAN269MEO15	15.3	69.9	14.8

3.2 Experiment Setup

Tests were carried out in both metal and ceramic reactors where continuous flow of liquid propellant was injected via a stainless steel syringe driven by a high-pressure syringe pump manufactured by Harvard Apparatus. A DC voltage was applied across the electrolytic channel in constant voltage mode by Agilent 6674A which could provide up to

60 VDC and 35 A. Power supply was always turned on before any liquid propellant was injected into the reactor to prevent the accumulation of liquid inside the channel which might lead to a sudden expansion of gases. The velocity of the liquid flow inside the channel in LTCC reactors with a flow rate of 800μl/min was 7.05×10^{-3} m/s and had a residence time of 4.68 seconds assuming the propellant remained in liquid phase throughout the channel. By assuming an equilibrium composition from HAN decomposition of only H_2O, N_2, and O_2 at 300°C, the velocity of the gaseous product inside the channel is 22.75 m/s with Re=484 and a residence time of 1.45×10^{-3} seconds assuming the whole channel was filled with gases at 300°C. A K-type (Omega.com) thermocouple with sheath diameter of 0.02 inch was inserted at 0.322 inch downstream from the exit of the electrolytic channel to measure the reaction temperature. The response time of the thermocouple was reported to be less than 0.25 seconds from Omega.com. The exit temperature and the electric current supplied were monitored and recorded via a LabVIEW program. The data acquisition hardware utilized was a PCI 6024E card and a SCB-68 connector box both from National Instruments. The reaction product gas evolved throughout the electrolytic decomposition process was sampled and analyzed using FTIR instrument- Nicolet 670 spectrometer from Thermo Scientific Company. A simplified schematic drawing of experimental setup is shown in Figure 3.1.

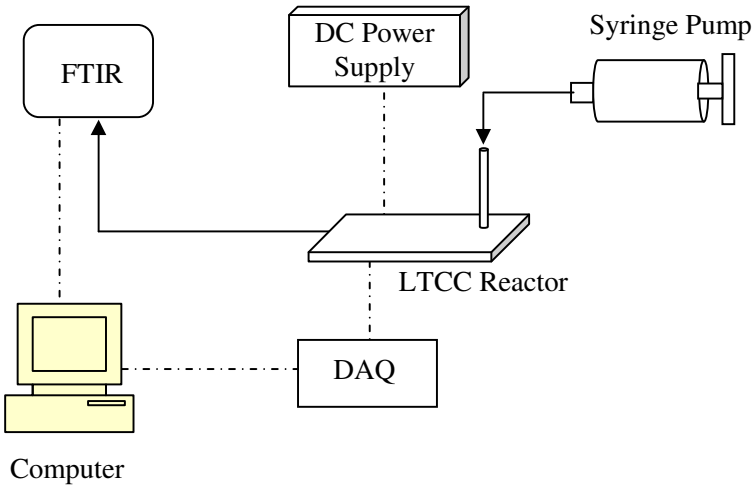

Figure 3.1 Schematic drawing for test setup of low temperature co-fired ceramic (LTCC) reactor

Combined electrolytic and catalytic ignition tests of HAN-based propellants were also performed. The warm electrolytic decomposition product was passed through a small catalyst bed to initiate the second stage reaction. The catalyst under investigation was 25-30 mesh S 405 which consists of Iridium (31-33%) as the active material deposited on alumina substrate manufactured by Aerojet.

3.3 Low Temperature Co-fired Ceramic (LTCC) Reactor

Low temperature co-fired ceramic tapes were originally developed as a multilayer ceramic technology for microelectronic packaging especially in telecommunication systems because of it superior microwave performance in addition to its good thermal and mechanical properties [36]. Having a faster and cheaper development process over traditional silicon microfabrication, LTCC technology has recently been utilized to develop microsensors, microactuators, microfluidic systems, and microthrusters [37-38].

In the process of manufacturing a LTCC system, each individual layer is processed separately in its unfired phase which is called "green tape." Desired configurations such as vias, cavities, and channels can be formed by cutting out the shapes in each layer utilizing punching, laser-cutting or CNC machining. A conductor can then be patterned onto the layers by screen printing and via filling. After processing each layer, the tapes are stacked together and laminated into a single rigid structure by applying pressure and heat prior to firing at higher temperatures. In the firing process, a ramped temperature profile is used to raise the temperature of the specimen to the LTCC sintering temperature, generally ranging from 850^{o}C to 1000^{o}C. During the process, the organic binder is initially oxidized and gasified at an intermediate temperature and at the highest temperature, the LTCC system, including the ceramic tapes and conductor, is sintered to attain full density of the ceramic specimen.

The LTCC tapes consist of composites of glass and ceramic, crystallized glass, composites of crystallized glass and ceramic, or liquid-phase sintered ceramics. The composites of glass and ceramic (usually alumina) system are the most commonly used [39]. The physical and electrical properties of the material could be adjusted by using different materials.

In addition to the advantages mentioned above, the capability and ease of handling both electrical and fluid functions in the system make LTCC technology a suitable manufacturing method for our application as an electrolytic reactor. The LTCC tape utilized in the current work is Dupont 951 Green Tape^{TM} with a thickness of 254 μm. Some of the mechanical and thermal properties are shown in Table 3.1.

Table 3.2 Some thermal and mechanical properties for Dupont 951 Green Tape ™

X,Y shrinkage (%)	12.7 ± 0.3
Z shrinkage (%)	15 ± 0.5
Density, (g/cm^3)	3.1
TCE (25 to 300°C), ppm/°C	5.8
Thermal Conductivity, W/m-K	3.3
Max. Operating Temperature, K	~1200
Flexural Strength, MPa	320
Young's Modulus, GPa	120

3.3.1 Design and Fabrication

The electrolytic reactor is composed of an electrolytic channel and combustion chamber where a catalyst can be placed inside and a thermocouple can be inserted. The schematic drawing for the LTCC reactor is shown in Figure 3.2. The width of the channel is 2.2 mm, the height is 0.86 mm, and the length is 33 mm. As for the combustion chamber, the width of the channel is 5.76 mm, the height is 1.73 mm, and the length is 10.15 mm. Ceramic tubing (1/16 inch in diameter), which serves as the inlet for fuel, is bonded to the reactor with ceramic putty based on silicate. The exhaust ceramic tubing (1/4 inch in diameter) is also attached to the exit of the reactor for product sampling purpose.

The fabrication process starts with cutting the "green tapes" with a thickness of 254μm for each layer into the desired profiles, i.e. electrolytic channel, combustion chamber, and vias. The machining method chosen here to cut the green tapes was laser cutting. The width of cutting line of the current laser machine was ~50μm. After machining the desired configurations, the electrodes and connecting wires were painted manually with platinum and silver paste and vias were filled with silver paste. The tapes were then stacked together with alignment pins on a platform. A viscous organic fluid which consists of 85wt% honey and 15wt% water was applied between each layer to bind the layers together before firing so that lamination under cold temperature and low pressure could be utilized to prevent the collapse of internal channels and the chamber from occurring. Carbon sacrifice layers which were completely burned out of the specimen at 600°C, were also used to ensure the integrity of the cavity structure during the lamination process.

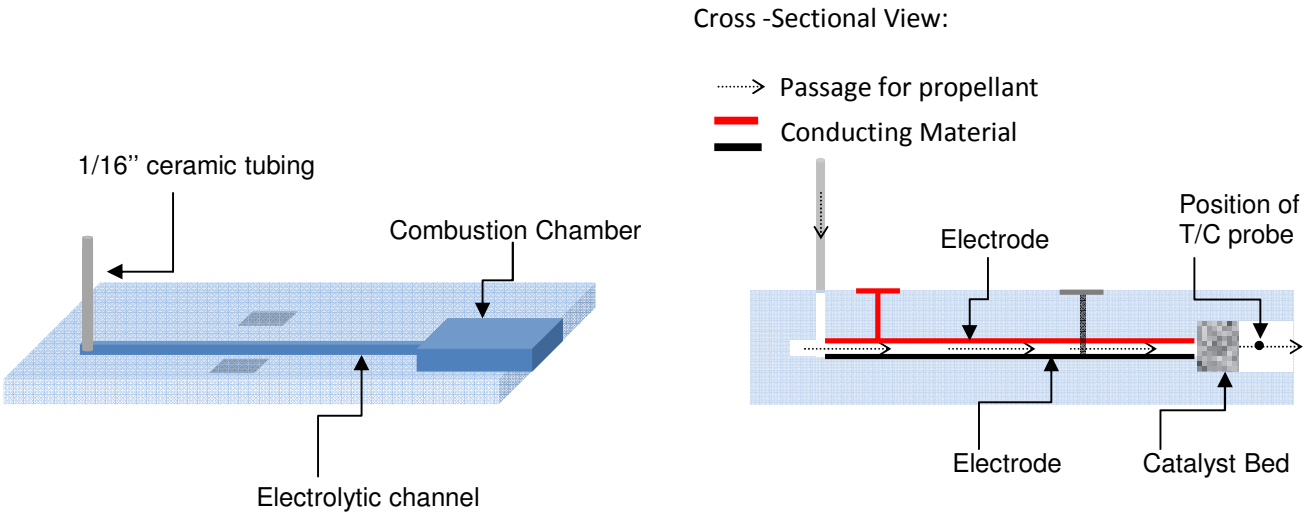

Figure 3.2 Schematic drawing for the LTCC reactor

3.4 Metal (Stainless Steel 316) Reactor

An optically-accessible electrolytic reactor as shown in Figure 3.3 has been designed and fabricated. The body of reactor is made of stainless steel 316 and the window mounted on two sides of reactor body is made of fused-silica. A pair of titanium electrodes with Teflon insulations was mounted on top and bottom of the reactor. The surface of the titanium electrodes was coated with platinum via electroplating to provide a better corrosion resistance.

The dimension of the electrolytic channel is 0.5 mm (height) x 3.69 mm (width) x 37.0 mm (length). The height of the channel (i.e. spacing between electrodes) could be increased by adding gasket. The exit of electrolytic channel is connected with a reaction chamber (ϕ=3 mm) where a catalyst can be loaded.

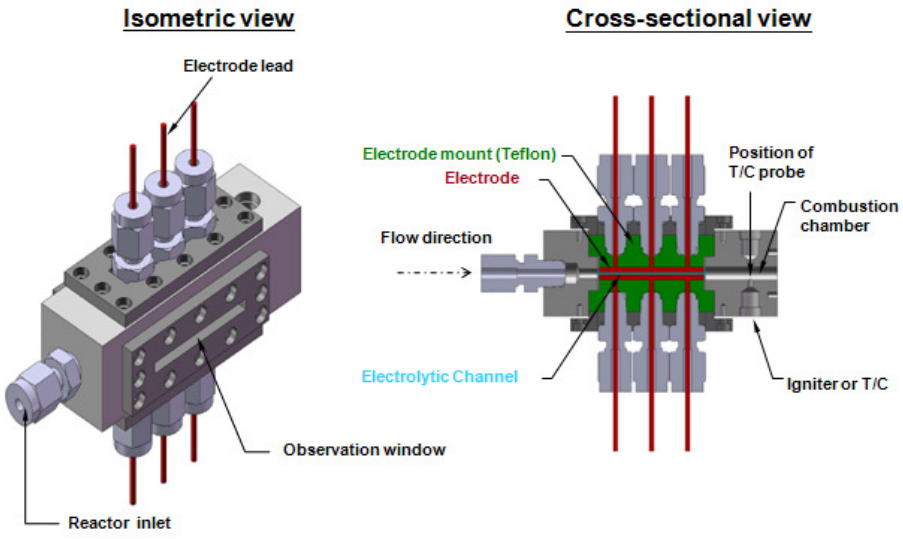

Figure 3.3 Schematic drawing of the electrolytic reactor

3.5 Species Measurement via Fourier Transform Infrared Spectrometry (FTIR)

The product gases from electrolytic decomposition of HAN-based propellants were sampled at the exit of the reactor and analyzed via FTIR. The product gases were firstly passed through a liquid trap where the species inside the product gases having a lower boiling point were condensed to keep liquid especially nitric acid from entering into the gas cell and depositing on the CaF_2 windows of the gas cell. The remaining gases were then diluted with nitrogen and directed into the gas cell of FTIR. A schematic drawing of the product sampling line is shown in Figure 3.4.

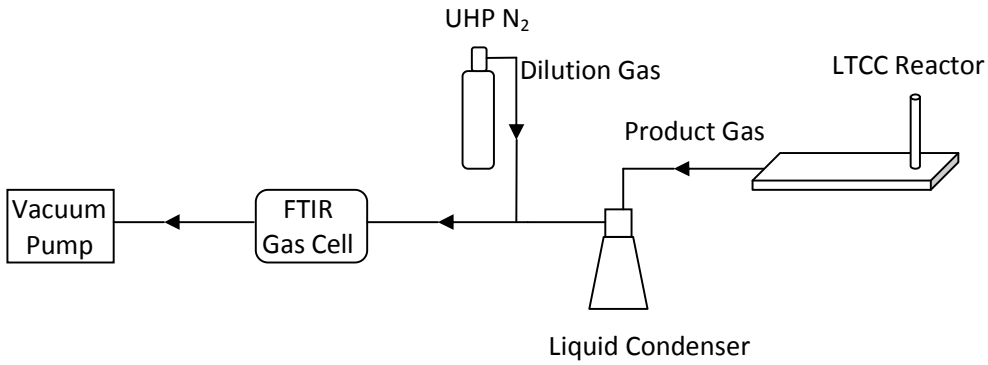

Figure 3.4 Schematic drawing of the reaction product sampling line

Fourier transform infrared spectrometry (FTIR) is one kind of infrared absorption spectrometry. The working principle of infrared absorption spectrometry is that when infrared light interacts with matters, the functional groups of matter absorb the infrared radiation with the same frequencies as their bonds or functional groups vibrate or rotate.

The species or the structures in molecules can thus be identified from the IR spectrum of the sample.

The principal components of the FTIR spectrometer include an IR light source, interferometer, detector, and sample compartment. Inside a Michelson interferometer which is the most commonly used interferometer in commercial FTIR instruments, there are one fixed window, one moving window and a beam splitter as shown in Figure 3.5. Infrared light is split through the beam splitter so that half of the light is transmitted to the fixed mirror and the other half is reflected to the moving mirror. The light is then recombined at the beam splitter again before it is passed through the sample. Because of the optical path difference, which is the difference in distance traveled by both beam lights before getting back to beam splitter, the recombined two beams can be out of phase and consequently interference occurs. Considering monochromatic light as an example, if the optical path difference is multiples of its wave length, the interference will then be constructive while if optical path difference is multiples of half of its wave length, the crests and troughs from the two beams will cancel so that the intensity of light is minimized. An interferogram is the plot of light intensity versus optical path difference which is changed by moving the mirror back and forth. For a broadband IR light source which emits light with a continuum of wavelength as in the FTIR instruments, the interferogram can be thought of as a summation of plots at each wave number. By performing the Fourier transform, the interferogram can be converted to an IR spectrum which is a plot of light intensity versus wavelength (or wavenumber).

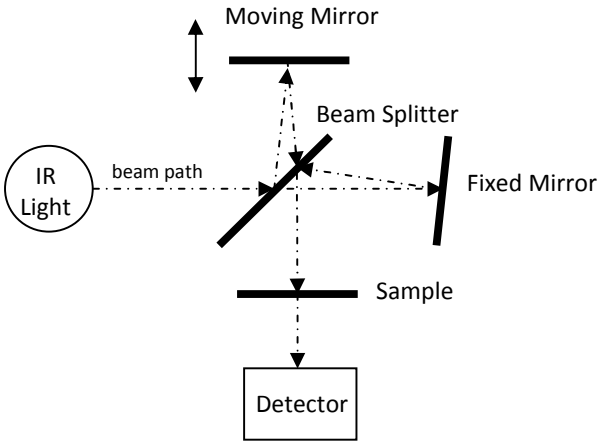

Figure 3.5An optical diagram of a Michelson interferometer

The spectrometer used in the current study was Nicolet 670 spectrometer from Thermo Scientific Company. The light source utilized is IR light and the detector equipped is a liquid nitrogen cooled mercury cadmium telluride (MCT-A) detector capable of receiving radiation from 650 to 4000 cm^{-1}. A 100 ml gas cell with 10 cm optical pathlength (Gemini Company) was installed in the sample compartment for gas analysis. CaF2 windows were used in the gas cell for transmission of IR light from 1000 to 4000 cm^{-1} because of its better resistance to acid. The temperature of the gas cell was maintained above 100^{o}C to ensure water did not condense in the gas cell. The pressure inside the gas cell was monitored and recorded and always maintained at ~9 psia for quantitative analysis. The product gas was diluted with ultra high purity nitrogen which is IR-inactive to lower the absorbance for improved quantification. In addition, the flush time of the gas cell was reduced because of a higher total flow rate.

The quantification of the FTIR measurement is based on Beer's law [40].

$$A = \varepsilon lc$$

Where A is absorbance, ε is absorptivity, l is pathlength, and c is concentration. Absorbance is defined as $A = \ln T$, where $T = \frac{I}{I_0} = \text{transmittance}$, I is the light intensity with a sample in the beam, i.e. the sample spectrum and I_o is the light intensity with no sample in the beam, i.e. the background spectrum. Absorbance is measured as peak height or peak area in the FTIR spectrum. Absorptivity is the proportionality constant between concentration and absorbance which is a property of a molecule changing with wavenumber. Pathlength is just the length that the IR beam travels in the gas cell. The concentration, c, is always in the units of moles/liter.

Chapter 4 Results and Discussion

Electrolytic decomposition of HAN-based propellants including 13M HAN and HAN269MEO15 was investigated in both ceramics and metal reactors for complementary types of experiments. The optically-accessible metal reactor was used for visual observation of the two-phase flow in the electrolytic channel and the LTCC reactors were used to study the overall process of the electrolytic decomposition. The difference in characteristics of the reaction temperature was identified between metal and LTCC reactors. To better understand the characteristics of electrolytic decomposition of HAN-based propellants, the evolution of reaction temperature, electric current, and product species, and visual observation were measured. Tests have been carried out including the electrolytic decomposition 13M HAN and HAN269MEO15. In addition to the low-temperature electrolytic decomposition, catalyst was also utilized in combination with electrolysis to trigger a high temperature reaction from room temperature.

4.1 Electrolytic Reactor in Single Channel Liquid Flow Reactors

In electrolytic decomposition of HAN-based propellant, condensed-phase reaction was initiated once the liquid propellant was pumped into the electrolytic channel where voltage was applied. The condensed-phase reaction generated gases quickly and brought the gas-phase temperature at the combustion chamber adjacent to the electrolytic channel up to around 100-120^{o}C at the same time. In the LTCC reactors, the gas-phase reaction continued to proceed in the combustion chamber after the condensed-phase reaction and

further raised the reaction temperature to 250-300^{o}C. However, for those experiments performed in the metal reactor, the steady-state reaction temperature measured at the combustion chamber was always confined between the water boiling point and the decomposition temperature of HAN (~120^{o}C). Due to the heat loss to the bulky structure, the reaction had not been able to overcome the barrier of water evaporation and the endothermic condensed-phase reaction to raise the temperature to a higher level within the duration of 2-3 minutes. The comparison of typical temperature profiles in the LTCC and metal reactors is shown in Figure 4.1.

Based on the different operational features of metal and LTCC reactors, the reactors were used for complementary types of experiments. LTCC reactors were used to study how the gas-phase reaction proceeded after the condensed-phase reaction while the metal reactor was used for visual observation of the two-phase flow in the electrolytic channel. Both reactors were operated at atmospheric pressure. In addition, both reactors could be designed with restrictions at the combustor exit to be operated at high pressures.

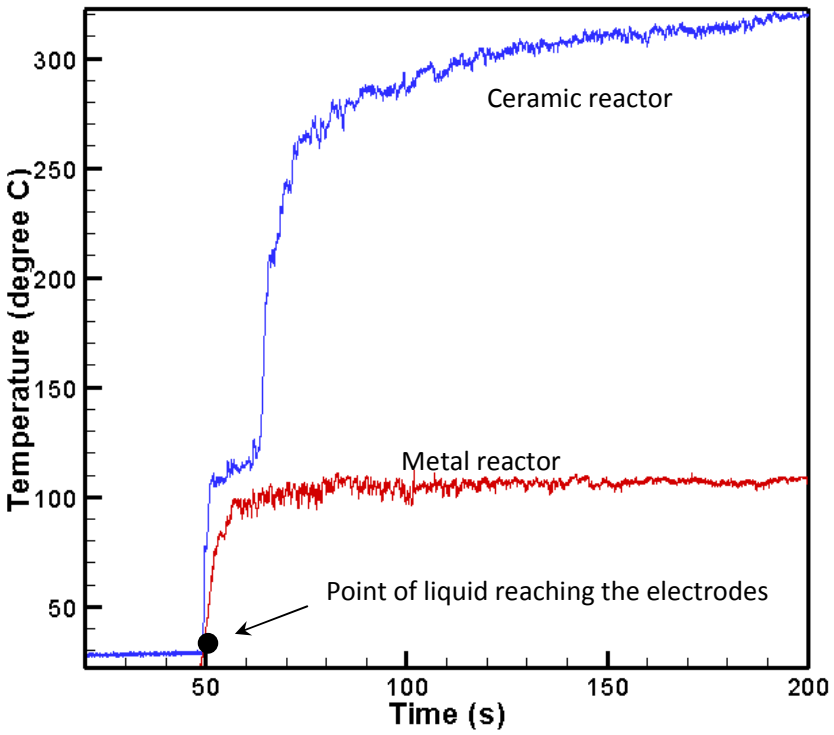

Figure 4.1 The comparison of temperature versus time profiles for LTCC and metal reactors

4.2 Decomposition of 13M HAN

4.2.1 Electrolytic decomposition of 13M HAN in the LTCC reactor

4.2.1.1 The Evolution of Temperature and Species

The process of electrolytic decomposition of 13M HAN in LTCC reactors could be divided into three segments by the slope break points of the temperature profile. In addition, the slope break points of species concentration corresponded roughly to those of the temperature profile suggesting a change of reaction mechanism at each segment. A typical temperature profile and species evolution in the electrolytic decomposition of

13M HAN are shown in Figure 4.2. The voltage applied was 30 VDC and the flow rate was 800µl/min.

The first segment is where the liquid-phase reaction takes place. The condensed-phase reaction occurs at room temperature once the liquid propellant entered the electrolytic channel, providing a closed circuit between the electrodes, where voltage was applied. The temperature at the combustion chamber rose up to above 100^{o}C followed by a short plateau at ~110^{o}C which agrees with the maximum liquid temperature measured by Risha et al. [29] in the steady state self decomposition of XM46 after the initiating electric energy was turned off. The major species, including N_2O, NO, and NO_2, quickly evolved during this segment and both N_2O and NO peaked at the end of this reaction segment. With the continuous supply of electric energy, the liquid-phase reaction can be maintained regardless of the heat loss in the system at the constant pressure of 1 atm. The energy released from the exothermic condensed-phase reaction was then used to initiate gas-phase reaction inside the combustion chamber. If the heat loss is minimized, for example, in the LTCC reactor versus the metal reactor, the reaction can continue for a short period of time after the applied voltage is removed at atmospheric pressure as shown in Figure 4.3. However, without the input of electric energy, most of the reaction energy from the first-stage reaction, i.e., HAN reaction, will be consumed as latent heat to evaporate the water. In such cases, heat loss in the LTCC system might appear to be significant compared to the sensible heat as can be seen from Figure 4.4 the decrease in temperature after the electric energy was removed.

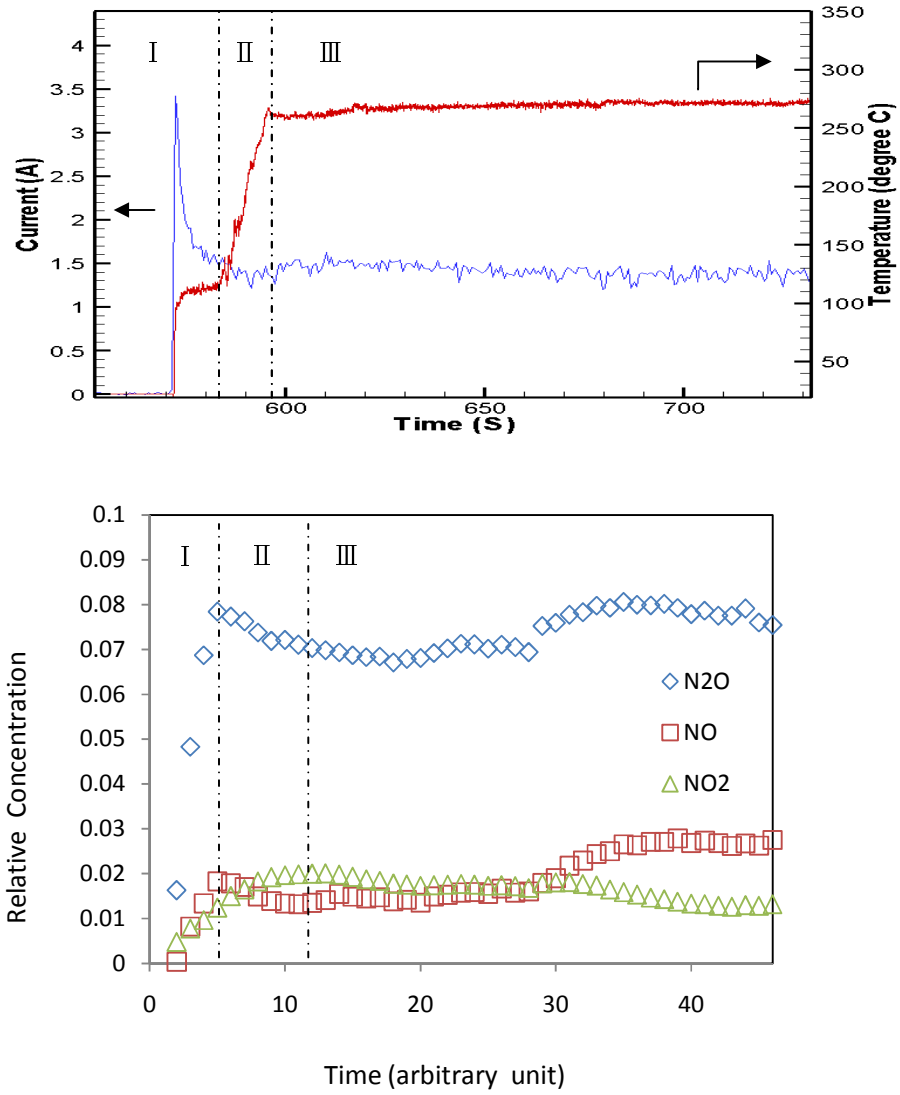

Figure 4.2 A typical temperature profile and the corresponding species evolution for electrolytic decomposition of 13M HAN

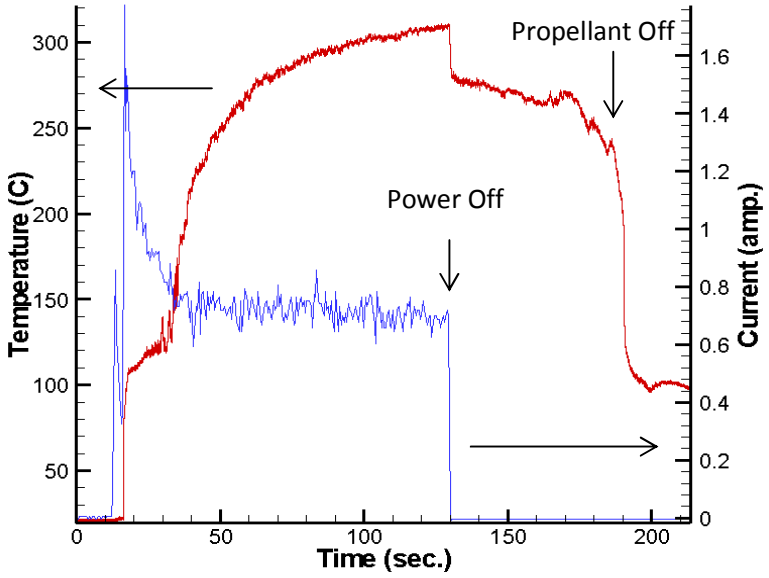

Figure 4.3 A typical temperature profile for electrolytic decomposition of 13M HAN showing that the reaction continued after the power was removed

During the second stage of reaction, the temperature rose quickly above 250°C suggesting the occurrence of exothermic gas-phase reaction. The delayed peak of NO_2 compared to that of N_2O and NO was believed to be relevant to the exothermic reaction. Both Cronin and Brill [20] and Lee and Litzinger [21] attributed the late appearance of NO_2 from the decomposition of HNO_3 in the thermolysis of HAN. An exotherm corresponding to the late appearance of NO_2 was also observed by Cronin and Brill [20]. After the rapid rise in temperature to 270°C, the reaction temperature attained a steady value. However, the decline of NO_2 and growth of NO which was always observed in this stage could be attributed to the decomposition of NO_2 into NO and O_2 which usually occurs at a measurable rate higher than 200°C [41] with the stoichiometry:

$$2NO_2 = 2NO + O_2 \qquad \text{(R 4-1)}$$

When the reaction rate was faster, which usually happened when a higher voltage (40 volts) was applied as shown in Figure 4.4, the individual reaction stages were not discernible. In addition to operating conditions, the fabrication process especially how well the conducting material was applied to the surfaces of LTCC reactors could affect the performance and efficacy of electrolytic decomposition since the reaction was initiated on the surface of anode and cathode.

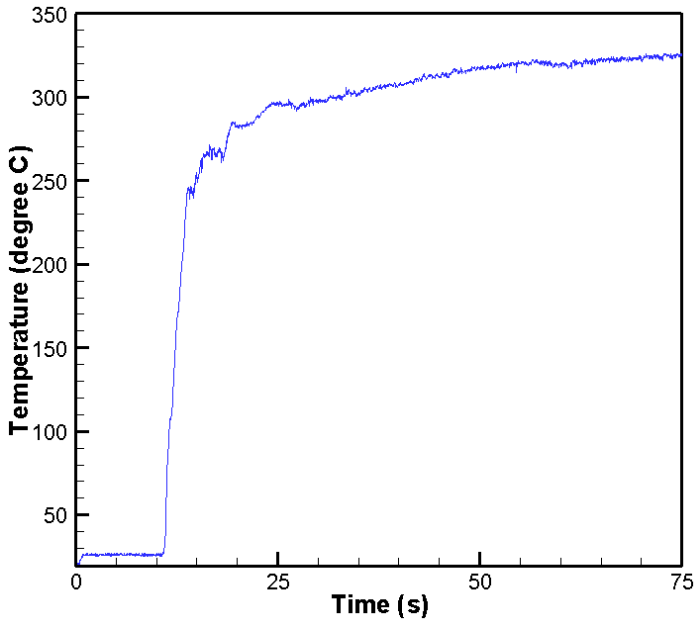

Figure 4.4 The rapid evolution of temperature in electrolytic decomposition of 13M HAN when a higher voltage was applied

As can be seen from Figure 4.2-4.4, the fastest temperature rise throughout the reaction process was at the beginning of segment 1 from room temperature to the plateau confined by water boiling point and HAN thermal decomposition point. The time required for the rapid rise of temperature was always of the same order of magnitude as the response

time for the thermocouple utilized, i.e., 0.25 seconds as mentioned in Chapter 3 or even equal or less to that under some cases. Consequently, slightly improved resolution in temperature may be obtained with a thermocouple having a smaller dimension at the junction.

4.2.1.2 The Evolution of Electric Current

The evolution of electric current throughout the decomposition process can be seen in Figure 4.2 and Figure 4.3. An overshoot at the early transient state was always observed. The overshoot in current can be explained by that liquid fills the electrolytic channel forming a close loop for electrons to pass through as the liquid reaches the channel. As the reaction proceeds, the liquid starts to bubble and forms gases such that the liquid remaining in the channel decreases and so does the electric current passage. A steady state value of electric current can be attained after the overshoot.

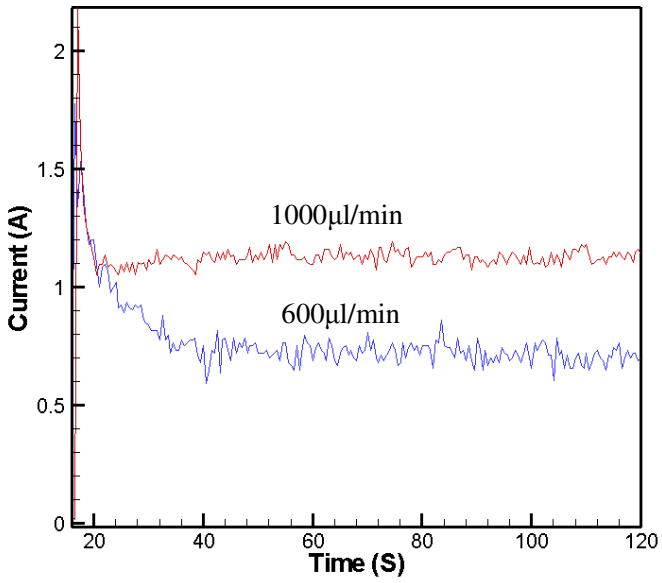

Figure 4.5 The comparison of the evolution of electric current of different flow rates

The effect of flow rates on the steady state value of electric current can be seen in Figure 4.5 that a higher flow rate can induce a higher steady state value of electric current in that in order to get a similar residence time inside the electrolytic channel for the liquid to be electrolytically decomposed into gases, the higher flow case needs a longer length since it has a higher velocity. In other words, more liquid remains in the channel at steady state for the higher flow rate case and so the passage of electric current is higher.

4.2.1.3 Visual Observation of Electrolytic Decomposition

Visual observation was made inside the electrolytic channel utilizing Phantom V7 high-speed camera with a framing rate of 200 fps in the optically-accessible metal reactor as shown in Figure 4.6. A flow rate of 1000 μl/min 13M HAN which corresponds to the bulk liquid velocity of 6.02 mm/s inside the channel with a voltage of 30 VDC was used. The edges of the channel were highlighted by green lines. The picture at the left was taken near the exit of the channel during the reaction. The clear channel suggests that most liquid was already decomposed into gases before reaching this section. The picture at the right was taken in the middle of channel entrance and exit. The bubbles could be seen throughout this section indicating the gases started to be formed from the liquid propellant.

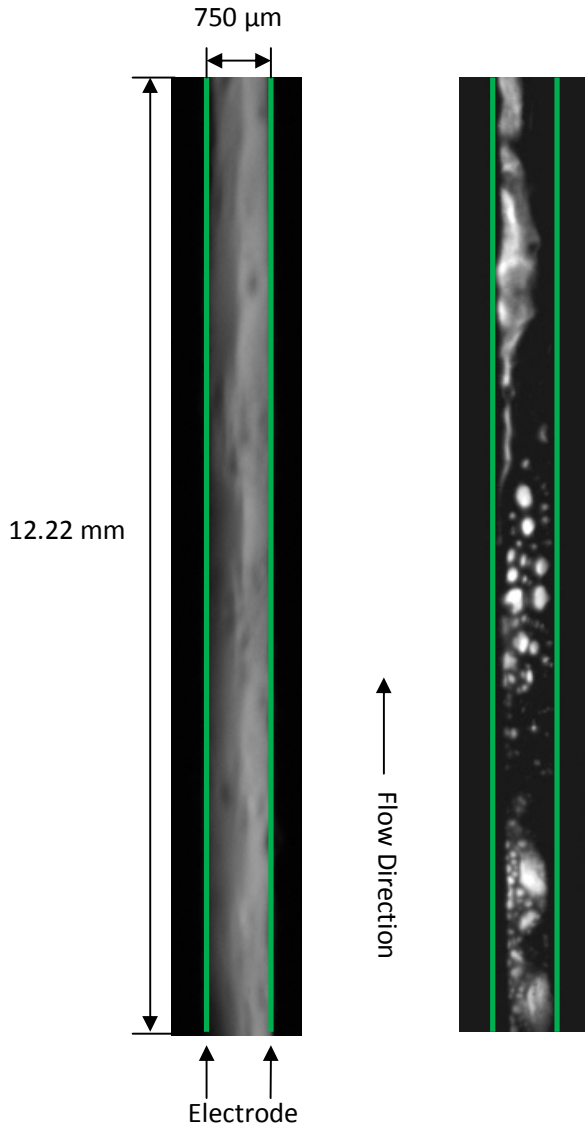

Figure 4.6 Pictures taken in the electrolytic channel via high-speed photography

Left: Near the exit (25.4 mm from the inlet to the channel);

Right: Middle section (12.7 mm from the inlet to the channel)

4.3 Electrolytic Decomposition of HAN269MEO15

The major species detected during the electrolytic decomposition of HAN269MEO15 were N_2O and CH_3ONO. These two species evolved in a similar way as shown in Figure 4.7. Methyl nitrite (CH_3ONO) evolved at an early stage of the reaction and was formed from the reaction between methanol and HAN/ products of HAN decomposition which was not seen in 13M HAN decomposition. Some reactions will be suggested for the formation of CH_3ONO in the following section.

The IR absorbance bands of NO_2 overlapped with the strong peaks of CH_3ONO and thus were difficult to identify. However, after close observation, NO and NO_2 were found present in only small amounts in the product gases compared to that found in the products gases from 13M HAN electrolysis and hence were not quantified. In addition, CO_2 was observed in small concentrations suggesting that the reaction was not complete at the current conditions. The evolution rate of N_2O was found to be slower than that during electrolytic decomposition of 13M HAN indicating that formation of CH_3ONO_2 either competed with the formation of N_2O, NO_2, and NO or consumed those species.

Nelson and Va [43] proposed some reaction paths for the process of synthesis of methyl nitrite via the gas-liquid reaction of methanol and dinitrogen trioxide (N_2O_3) and the condensed-phase reaction of methanol and nitrous acid (HONO). The reaction paths were shown as follows:

$$CH_3OH_{(l)} + N_2O_{3(g)} \rightarrow CH_3ONO_{(g)} + HONO_{(l)} \qquad \text{(R 4-2)}$$

$$CH_3OH_{(l)} + HONO_{(l)} \rightarrow CH_3ONO_{(g)} + H_2O_{(l)} \quad \text{(R 4-3)}$$

Noteworthy is that (R 4-3) was referred to as instantaneous reaction.

Other reaction paths were also possible for the formation of methyl nitrite including gas-phase reaction between CH_3OH and NO_2 [44].

$$CH_3OH_{(g)} + NO_{2(g)} \rightarrow CH_3ONO_{(g)} + HNO_{3(g)} \quad \text{(R 4-4)}$$

The condensed-phase reaction between methanol and nitrous acid (R 4-3) is thought to be the most probable reaction path to form methyl nitrite in the current study. Nitrous acid is an important intermediate species formed from the product of the initiate proton transfer reaction ($NH_2OH + HNO_3 \leftrightarrow HONO + HNO + H_2O$) in the decomposition of HAN and it is responsible for the formation of N_2O, NO, and NO_2 as shown in Table 2.2. The consumption of nitrous acid during the formation of methyl nitrite can answer why N_2O was formed at a slower rate and only little NO and NO_2 was observed. The evidence supporting for the condensed-phase reaction between methanol and nitrous acid also comes from the early evolution of methyl nitrite in the reaction process since nitrous acid is an early intermediate product in HAN decomposition.

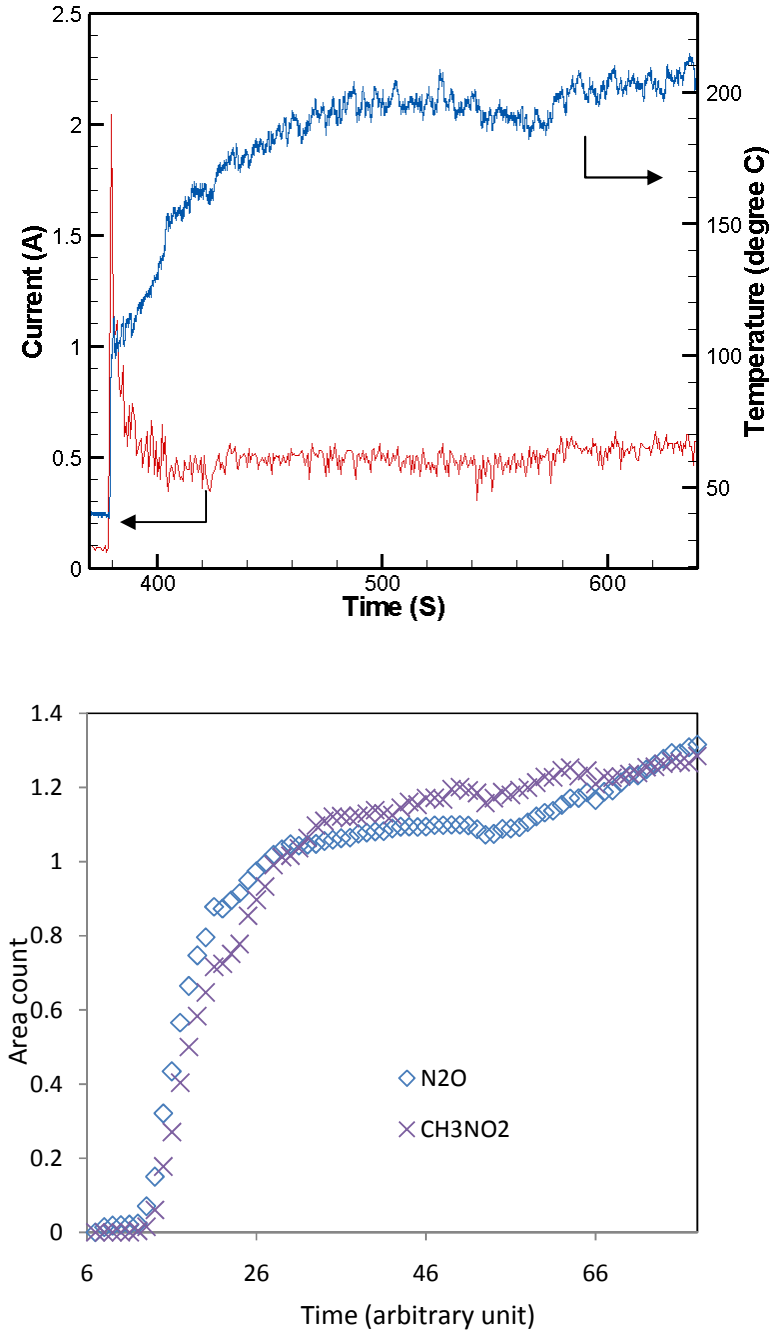

Figure 4.7 A typical temperature profile and the corresponding species evolution for electrolytic decomposition of HAN269MEO15

4.4 Combined- Electrolytic and Catalytic Ignition

The combined-electrolytic and catalytic ignition was demonstrated at atmospheric pressure to initiate a high temperature reaction which then became self-sustained. Catalyst was loaded into the combustion chamber to study the feasibility of combined-electrolytic and catalytic ignition of HAN-based propellants. The concept was to flow the warm gas (250-300^{o}C) produced from electrolytic decomposition through a catalyst bed to initiate the high temperature reaction of HAN269MEO15. Preheating of the catalyst would not be necessary as the gases passing over the catalyst would be at an elevated temperature (~300^{o}C) and consist of more reactive decomposed species compared to the original propellant.

The temperature profile taken during the combined process is shown in Figure 4.8 with test condition shown in Table 4.1. The applied voltage was removed once the reaction temperature reached 700^{o}C. The temperature initially dropped as the energy was removed, but then increased steadily to become a self-sustained reaction. The injection of propellant was stopped before the temperature reached the maximum operating temperature of the LTCC material. Experiments have also been performed in a reactor with only 10 mg of catalyst loaded. Under such cases, the temperature rose slowly and dropped after the power was shut-off because the energy released from the catalytic reaction was not able to cover the heat loss and the activation energy required for the reaction. Because of the fast rise in temperature in the LTCC reactor, cracking of the

LTCC reactor in combined-electrolytic and catalytic reaction was always observed near the juncture of the electrolytic channel and catalyst chamber. To overcome the material limitations of the LTCC tapes, high temperature co-fired ceramic tapes would be necessary. If the thermal shock is still too much for ceramics, metal reactors would be required.

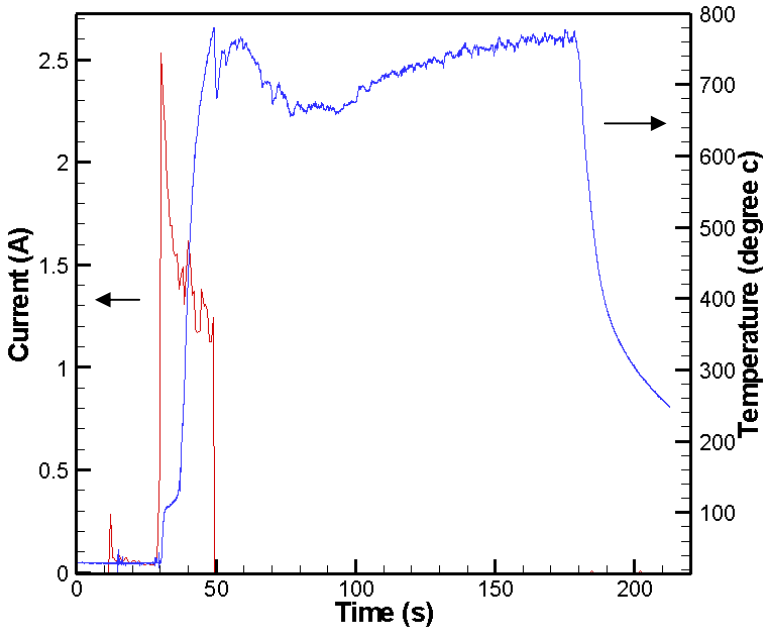

Figure 4.8 Temperature profile for combined- electrolytic and catalytic ignition of HAN269MEO15

Table 4.1 Operating conditions for test shown in Figure 4.8

Propellant	HAN269MEO15
Flow Rate	800 µl/min
Catalyst	58 mg of S 405
Electrolytic Voltage	30 VDC
Chamber Pressure	Open to atmosphere

4.4.1 Species Evolution for Combined- Electrolytic and Catalytic Reaction of HAN269MEO15

Chemical analyses were performed on the product gases from the combined electrolysis and catalytic reactor. The temperature profile and species evolution are shown in Figure 4.9 and Figure 4.10 with the test conditions shown in Table 4.2. The entire reaction process could be seen as the combination of electrolysis-dominated decomposition followed by catalytic reaction. During stage I shown in Figure 4.9, the reaction is similar to electrolytic decomposition of HAN269MEO15 where N_2O and CH_3ONO evolved quickly. Other gases like NO, NO_2, CO and CO_2 were only present in a small amount. As the temperature rose further during stage II, the catalytic reaction dominates. The consumption of N_2O and CH_3ONO and the formation of CO_2, CO, and NO suggests a more vigorous reaction occurred in the combustion chamber. The concentration of those species then started to level off as well as the reaction temperature during stage III. NO is an important intermediate product in the oxidation or thermal decomposition of CH_3ONO [45, 46]. As can be seen in Figure 4.10, NO was the major nitrogen containing species among the IR active gases identified. If the reactor was operated at higher pressure (or an even higher temperature), the NO would be expected to be reduced to N_2 releasing more energy.

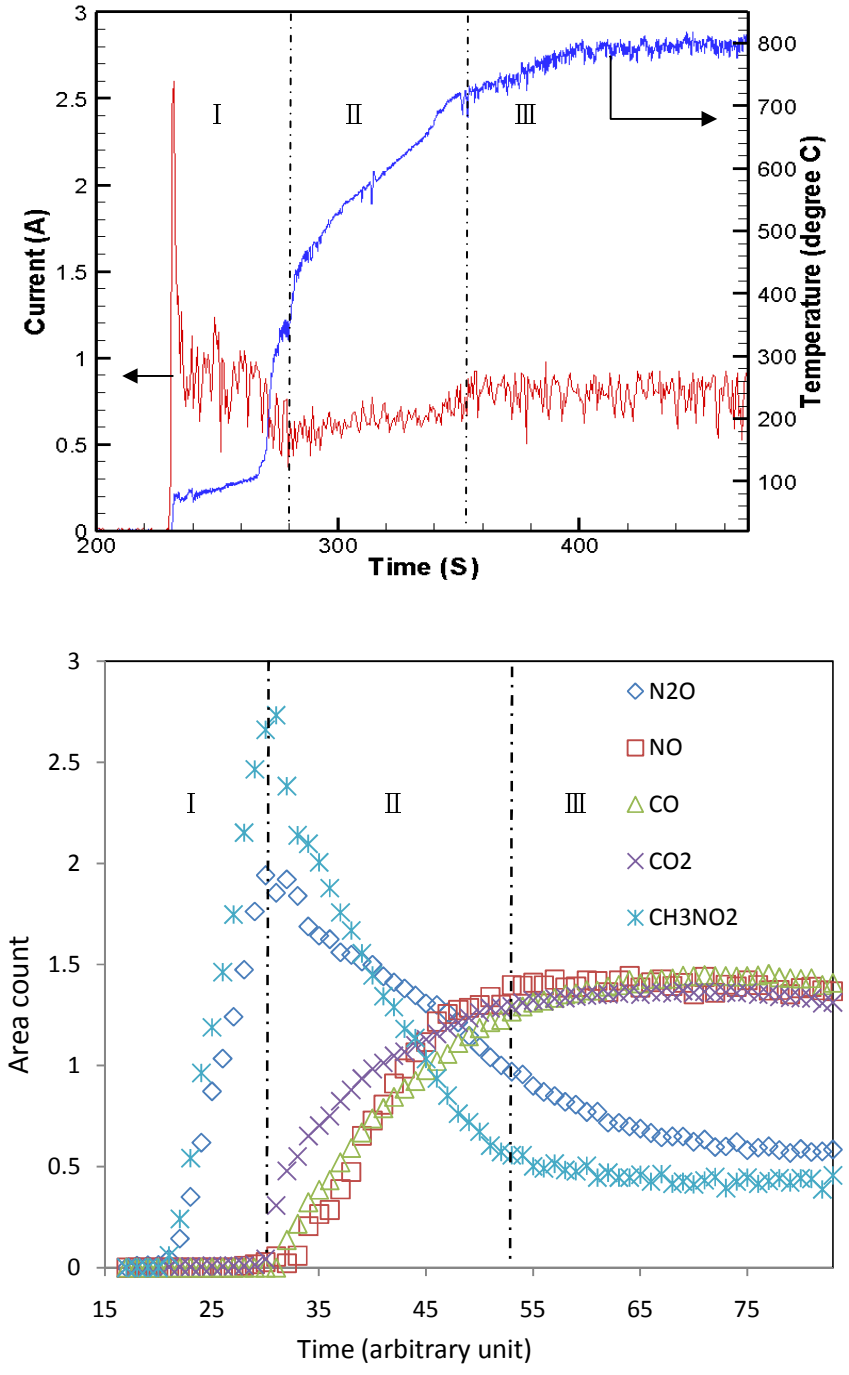

Figure 4.9 A typical temperature profile and the corresponding species evolution for combined-electrolytic and catalytic ignition for HAN269MEO15

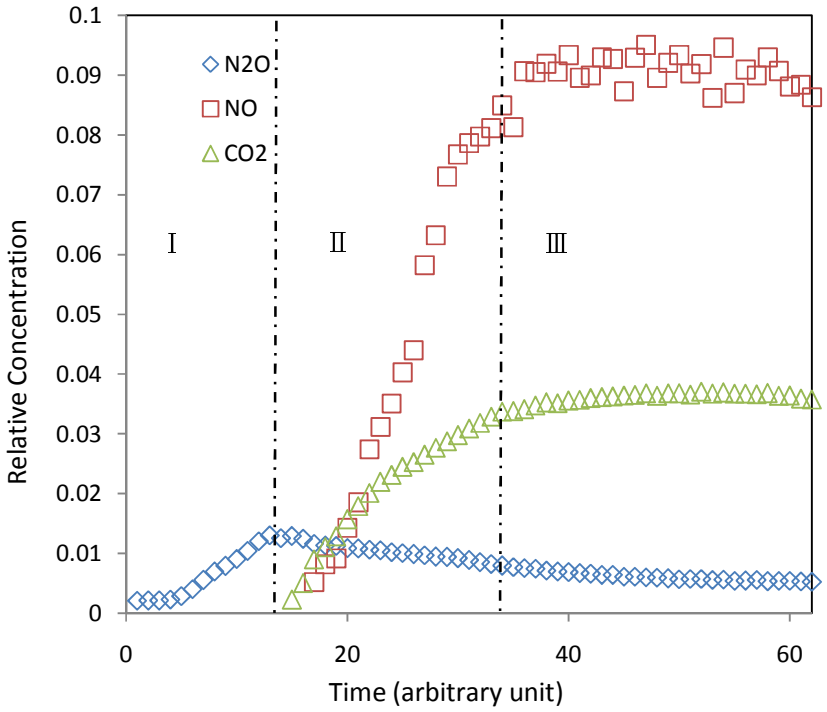

Figure 4.10 The species evolution in relative concentration for combined-electrolytic and catalytic ignition for HAN269MEO15

Table 4.2 Operating conditions for test shown in Figure 4.9

Propellant	HAN269MEO15
Flow Rate	600 µl/min
Catalyst	10 mg of S 405
Electrolytic Voltage	30 VDC
Chamber Pressure	Open to atmosphere

Chapter 5 Conclusion

5.1 Summary

The characteristics of electrolytic decomposition of HAN-based propellant were investigated in both metal and ceramic reactors. In LTCC reactors, the process of electrolytic decomposition of 13M HAN solution was found to be composed of three steps. The reaction was firstly initiated by condensed-phase reaction as the liquid propellant entered the electrolytic channel. The reaction temperature quickly rose to above 100^{o}C and then kept rising at a much slower rate. N_2O, NO, and NO_2 evolved quickly at this step. Note that the species in vapor phase were taken out before the species analysis and IR-inactive gases were not identified in the analysis. The next step is dominated by the exothermic decomposition which was thought to be relevant to the formation of NO_2 releasing more energy to raise the reaction temperature to ~250-300^{o}C. During the last step, the temperature achieved a steady-state value at ~300^{o}C and the conversion of NO_2 into NO occurred. For experiments performed in the optical metal reactor, however, only the condensed-phase reaction was observed due to the greater heat loss to the reactor structure. Electrolytic decomposition of HAN269MEO15 was also investigated in ceramic reactors. The temperature profiles were similar to those observed for 13M HAN solutions. The major species observed included N_2O and CH_3NO_2 (Methyl Nitrite) which evolved quickly at first with temperature and slowed down when the temperature started to level off.

The combined-electrolytic and catalytic ignition for HAN269MEO15 was demonstrated in LTCC reactor with catalyst S405 at atmospheric pressure. A maximum reaction temperature of around 800^{o}C was measured. The ability to initiate the decomposition of HAN-based propellant at room temperature would make electrolytic decomposition beneficial under the circumstances when preheating is not desirable. The process of combined-electrolytic and catalytic ignition can be envisioned as the combination of electrolytic decomposition and catalytic ignition of the gaseous products evolved from electrolysis. The electrolytic decomposition initiated the reaction and dominated at a lower temperature. The major species observed during this stage was very much like that from the electrolytic decomposition of HAN269MEO15 including N_2O and CH_3NO_2. As the temperature increased, catalytic combustion dominated the overall reaction where much of CO_2, CO, and NO were produced. However, combustion remained incomplete as indicated by the presence of NO and a much lower reaction temperature of 800^{o}C compared to the adiabatic flame temperature of HAN269MEO15 of 1929^{o}C. High pressures are generally necessary for NO reduction in short residence times. Hence pressurization in motor combustion chambers would improve the overall efficiency.

5.2 Future Work

Some of the important characteristics of electrolytic decomposition of 13M HAN and HAN269MEO15 were identified in the current study. However, the initiate reaction in condensed-phase still needs further investigation. The identification of species from the liquid condensed during reaction, the detection of oxygen and hydrogen which are important products in water electrolysis and the capability for resolving species evolution during transient state can help further understand the reaction process.

In addition, finding an optimized operating condition for electrolytic decomposition of HAN-based propellants which could not only shorten the ignition delay but also minimize the energy consumption is of great importance to its application in microthruster ignition. Possible approaches include: (a) exploration in different fuel blends which might expedite the electrolytic reaction such as ionic fuels with better electrical conductivity, (b) the addition of grapheme also could enhance the electric conductivity and possibly serve as catalyst, and (c) performing parametric studies including the effect of dimension of the channel, an optimized flow rate corresponding to the size of the channel, voltages applied…etc.

References

1. Micci, M.M. and Ketsdever, A.D., eds., "Micropropulsion for Small Spacecraft", Progress in Astronautics and Aeronautics, Vol. 187, AIAA.
2. Hill, P. and Peterson, C., "Mechanics and Thermodynamics of Propulsion," 2nd Edition, Addison-Wesley.
3. Yetter, R.A., Yang, V., Wu, M.H., Wang, Y., Milius, D., Aksay, I.A., and Dryer, F.L., "Combustion Issues and Approaches for Chemical Microthrusters,"6thInternational Symposium on Special Topics in Chemical Propulsion, Santiago, Chile, 2005.
4. Reed, B.D., "On-Board Chemical Propulsion Technology, " Tenth International Workshop on Combustion and Propulsion, La Spezia, Italy, September, 2003
5. Schmidt, E.W. and Wucherer, E.J., "Hydrazine(s) vs. Nontoxic Propellants-Where Do We Stand Now?" Proc. '2nd Int. Conference on Green Propellants for Space Propulsion,' Cagliari, Sardinia, Italy, June, 2004
6. Meinhardt, D., Brewster, G., Christofferson, S., and Wucherer, E. J., "Development and Testing of New, HAN-Based Monopropellants in Small Rocket Thrusters," AIAA Paper 98-4006, Jul. 1998.
7. Wucherer, E. J., Christofferson, S. S., and Reed, B., "Assessment of High Performance HAN-Monopropellants," AIAA paper 2000-3872, Jul. 2000.
8. Lube, D. M., Wucherer, E. J., Reed, B., "Evaluation of HAN-Based Propellant Blends," AIAA Paper 2003-4643, Jul. 2003.
9. Klein, N., "Liquid Propellants for Use in Guns," Gun Propulsion Technology, Progress in Astronautics and Aeronautics, edited by Ludwig Stiefel, Vol. 109, AIAA, Chapter 14.

10. Klein, N., “Ignition and Combustion of the HAN-Based Liquid Propellants, ”Proceedings of 27th JANNAF Combustion Subcommittee Meeting, CPIA Pub.557, Vol. 1, Chemical Propulsion Information Agency, Laurel, MD, 1990, pp.443-450.

11. Vosen, S. R., “The Burning Rate of Hydroxylammonium Nitrate-Based Liquid Propellants,” 22nd Symposium (International) on Combustion, Combustion Institute, Pittsburgh, PA, 1988, pp. 1817-1825.

12. Vosen, S. R., “Hydroxylammonium Nitrate-Based Liquid Propellant Combustion – Interpretation of Strand Burner Data and the Laminar Burning Velocity,”Combustion and Flame, Vol. 82, Nos. 3-4, 1990, pp. 376-388

13. Chang, Y.-P., Boyer, E. and Kuo, K. K., “Combustion Behavior and Flame Structure of XM46 Liquid Propellant,” Journal of Propulsion and Power, Vol. 17, No. 4, July 2001, pp. 800-808

14. Chang, Y.-P., and Kuo, K. K., “Assessment of Combustion Characteristics and Mechanism of Hydroxylammonium Nitrate-Based Liquid Monopropellant,” Journal of Propulsion and Power, Vol. 18, No. 5, September 2002, pp. 1076-1085

15. Chang, Y.-P., Josten, J. K., B. Q. Zhang, Kuo, K. K., Reed, B. D. “Combustion Characteristics of Energetic HAN/Methanol-Based Monopropellants,” AIAA paper 2002-4032, July 2002

16. Lee, Y. J. and Litzinger, T. A., “Combustion Chemistry of HAN, TEAN, andXM46,” Combustion Science and Technology, Vol. 141, Nos. 1-6, 1999, pp. 19-36.

17. Chang, Y.-P., “Combustion behavior of HAN-based propellants,” PhD Thesis, The Pennsylvania State University, 2002

18. Klein, N. and Leveritt, C. S., “Methods for Evaluation of Thermally Induced Reactions in

Liquid Propellants," BRL Technical Reports, BRL-TR-3069, December, 1989.

19. Courthéoux, L., Eloirdi,- R.,Rossignol, S.,Kappenstein, C.,Duprez, D.,andPillet, N., "Catalytic Decomposition of HAN-Water Binary Mixtures," AIAA paper 2002-4027, Jul. 2002.
20. Cronin, J. T. and Brill, T. B., "Thermal Decomposition of Energetic Materials 29– The Fast Thermal Decomposition Characteristics of a Multicomponent Material: Liquid Gun Propellant 1845," Combustion and Flame, Vol. 74, No. 1, 1988, pp. 81-89.
21. Lee, H. and Litzinger, T. A., "Thermal Decomposition of HAN-Based Liquid Propellants," Combustion and Flame, Vol. 127, No. 4, 2001, pp. 2205–2222
22. Wucherer, E. J., Cook, T., Stiefel, M., Humphries, R. and Parker, J., "Hydrazine Catalyst Production – Sustaining S-405 Technology," AIAA paper 2003-5079, Jul. 2003.
23. Courthéoux, L., Eloirdi, R., Rossignol, S., Kappenstein, C., Duprez, D., and Pillet, N., "Catalytic Decomposition of HAN-Water Binary Mixtures," AIAA paper 2002-4027, Jul. 2002.
24. DeSpirito, J and Knapton, J. D., "Electric Ignition of Liquid Propellant for use in Guns," Combustion Science and technology, Vol. 176, 1991, pp. 251-263
25. Ludwig Stiefel ed., "Gun Propulsion technology," Progress in Astronautics and Aeronautics, edited by, Vol. 109, AIAA
26. Russell S and Fondrk TL (1975) Monopropellant Electrolytic Igniter, United States .Patent #3,861,137, Jan. 21.
27. Carleton, F. B., Klein, N., Krallis, K., and Weinberg, F. J., "Laser Ignition of Liquid Propellants," Twenty-Third (International) on Combustion/ The Combustion Institute, pp.1323-1329

28. Yetter, R. A., Yang, V., Wang, Z., Wang, Y., Milius, D., Peluse, M., Aksay, I., Angiolletti, M., Dryer, F. L., "Development of Meso and Micro Scale Liquid Propellant Thrusters," AIAA paper 2003-0676, January 2003

29. Risha, G. A., Yetter, R. A., and Yang, V., "Electrolytic-Induced Decomposition and Ignition of HAN-based Liquid Monopropellants," 6th International Symposium in Chemical Propulsion, Santiago, Chile, 2005

30. Wu, M.H., Yetter, R.A., "A novel electrolytic ignition monopropellant microthruster based on low temperature co-fired ceramic tape technology," Lab on a Chip, Vol. 9, 2009 pp. 910-916

31. Oxley, J. C., Brower, K. R., "Thermal Decomposition of Hydroxylamine Nitrate," SPIE, Vol.872, 1988, pp.63-70

32. Lee, H. S. and Litzinger, T. A., "Chemical Kinetic Study of HAN Decomposition," Combustion and Flame, Vol. 135, 2003, pp. 151–169

33. Meng, H, Khare, P., Risha, G. A., Yetter, R. A., Yang, V., "Decomposition and Ignition of HAN-based Monopropellants by Electrolysis," AIAA Paper 2009-451, January 2009

34. Katsumi, T., Kodama, H., Matsuo, T., Ogawa, H., Tsuboi, N. and Hori, K., "Combustion Characteristics of a Hydroxylammonium Nitrate Based Liquid Propellant. Combustion Mechanism and Application to Thrusters," Combustion, Explosion, and Shock Waves, Vol. 45, No. 4, 2009, pp. 442–453

35. Wucherer, E. J., Cook, T., Stiefel, M., Humphries, R. and Parker, J., "Hydrazine Catalyst Production – Sustaining S-405 Technology," AIAA paper 2003-5079, Jul. 2003.

36. Buchanan, R. C., "Ceramic Materials for Electronics" 3rd edition, CRC press

37. Gongora-Rubio, M.R., Espinoza-Vallejos, P., Sola-Laguna, L., and Santiago-Aviles,

J.J."Overview of low temperature co-fired ceramics tape technology for meso-system technology (MsST)," Sensors and Actuators A, Vol. 89, 2001, pp. 222-241.

38. Golonka, L.J., "Technology and applications of Low Temperature Cofired Ceramic(LTCC) based sensors and microsystems," Bulletin of The Polish Academy of Sciences, Vol. 54, No.2, 2006
39. Imanaka, Y., **"**Multilayered Low Temperature Cofired Ceramics (LTCC) Technology," 2004, Springer
40. Smith, B. C., "Fundamentals of Fourier Transform Infrared Spectroscopy," 2000, CRC Press
41. Bamford, C. H. and Tipper C. F. H. eds., "Decomposition of Inorganic and Organometallic Compounds," Comprehensive Chemical Kinetics, Vol.4
42. Kim, E. S., Lee, H. S., Mallery, C. F., and Thynell, S. T., "Thermal Decomposition Studies of Energetic Materials Using Confined Rapid Thermolysis/ FTIR Spectroscopy," Combustion and Flame, Vol. 110, 1997, pp. 239-255
43. Nelson, J. R., and Va., W., "Process and reaction vessel for production of alkyl nitrite," United States Patent #4,908,466, 1990
44. Koda, S., Kota, Y., Okada, J., and Akita, K., "Reaction Kinetics of Nitrogen Dioxide with Methanol in the Gas Phase," Environ. Sci. Technol., Vol. 79, 1985, pp. 262-264
45. Arden, E. A. and Powling J, "The Methyl Nitrite Decomposition Flame," Combustion and Flame, Vol. 2, No.1, 1958, Pages 55-68
46. Gray, P., Hall, A. R., and Wolfhard, H. G., "Stationary Flames of Methyl Nitrate and Methyl Nitrite," Proceedings of the Royal Society of London. Series A, Mathematical and Physical Sciences, Vol. 232, No. 1190, pp. 389-403